Thiosemicarbazonecopper/Halido Systems: Structure and DFT Analysis of the Magnetic Coupling

Alondra Jiménez-Pérez [1], Sara Marcos-Gómez [1], Gotzon Madariaga [2,3], Manuel Zapico [1], Pablo Vitoria [4], Javier Tercero [5], M. Begoña Torres [6], Luis Lezama [4], José Vicente Cuevas [1], Iñigo Etxebarria [2,3] and Javier García-Tojal [1,*]

1   Department of Chemistry, University of Burgos, Pza. Misael Bañuelos s/n, E-9001 Burgos, Spain
2   Department of Physics, University of the Basque Country, P.O. Box 644, E-48080 Bilbao, Spain
3   EHU Quantum Center, University of the Basque Country, UPV/EHU, E-48080 Bilbao, Spain
4   Department of Organic and Inorganic Chemistry, University of the Basque Country, P.O. Box 644, E-48080 Bilbao, Spain
5   Department of Inorganic and Organic Chemistry, Faculty of Chemistry, Martí i Franquès 1-11, University of Barcelona, 08028 Barcelona, Spain
6   Departamento de Matemáticas y Computación, Escuela Politécnica Superior, Universidad de Burgos, ES-09006 Burgos, Spain
*   Correspondence: qipgatoj@ubu.es

Abstract: Experimental magnetic studies performed on the [{CuLX}$_2$] system (HL = pyridine-2-carbaldehyde thiosemicarbazone, X = Cl$^-$, Br$^-$, I$^-$) point to the larger electronegativity in X, the lower magnitude of the antiferromagnetic interactions. In order to confirm this and other trends observed and to dip into them, computational studies on the [{CuLX}$_2$] (X = Cl$^-$ (**1**), I$^-$ (**2**)) compounds are here reported. The chemical and structural comparisons have been extended to the compounds obtained in acid medium. In this regard, chlorido ligands yield the [Cu(HL)Cl$_2$]·H$_2$O (**3**) complex, whose crystal structure shows that thiosemicarbazone links as a tridentate chelate ligand to square pyramidal Cu(II) ions. On the other hand, iodido ligands provoke the formation of the [{Cu(H$_2$L)I$_2$}$_2$] (**4**) derivative, which contains pyridine-protonated cationic H$_2$L$^+$ as a S-donor monodentate ligand bonded to Cu(I) ions. Crystallographic, infrared and electron paramagnetic resonance spectroscopic results are discussed. Computational calculations predict a greater stability for the chlorido species, containing both the neutral (HL) and anionic (L$^-$) ligand. The theoretical magnetic studies considering isolated dimeric entities reproduce the sign and magnitude of the antiferromagnetism in **1**, but no good agreement is found for compound **2**. The sensitivity to the basis set and the presence of interdimer magnetic interactions are debated.

Keywords: chloro; coordination chemistry; copper; density functional theory; iodo; structure; thiosemicarbazone

1. Introduction

Molecular magnetism analyzes the influence of chemical composition and structure in the magnetic properties of organic and coordination compounds [1]. Focusing on cooperative magnetic phenomena, which are those established among interacting paramagnetic centers, two usual magnetic behaviors can be distinguished: ferromagnetism and antiferromagnetism. The simplest cooperative magnetic interactions are those involving two centers with S = 1/2 within an isolated centrosymmetric magnetic dimer. In this case, the ferromagnetic state will be S = 1, while S = 0 is the antiferromagnetic state. A prolific research has been performed on dimers containing Cu(II) ions due to the presence of only one unpaired electron in the 3d^9 electron configuration of each metal center (S = 1/2). The choice of the ligand is essential to confer simplicity and versatility to the system. Thus, a greater denticity in the Y ligand, which means a larger number of donor atoms in the

ligand, usually carries a structural uniformity for the rigid $[CuY]^{n+}$ fragments, at least to a certain extent. It allows a fine and easy chemical modulation in these systems, i.e., changes in the substituents, the ancillary ligands or the counterions. A good strategy is the use of tridentate ligands, which leads to 1–3 available positions for placing coligands, depending on the coordination number of the complexes (n = 4–6). A thoroughly explored, as much structurally as magnetically, dimer system containing Cu(II) ions linked to tridentate ligands is that derived from the pyridine-2-carbaldehyde thiosemicarbazone ligand (HL).

　　Thiosemicarbazones (TSCs) are organic molecules with azomethine (1), hydrazine (2) and thioamide (3) functional groups (see Scheme 1) [2–27]. In the case of HL, R_1 = pyridine (py) and $R_2 = R_3 = R_4 = H$ (Schemes 1 and 2). The deprotonation of HL occurs from the release of H^+ ions from the hydrazine N atom and yields the anionic L^- form (Scheme 2). This ligand usually exhibits a tridentate NNS behavior (see atoms with asterisk in Scheme 2) to give planar $[Cu(HL)]^{2+}$ or $[CuL]^+$ entities, depending on the neutral or anionic form of the TSC in the compound [28–32]. The $[Cu(HL)]^{2+}/[CuL]^+$ entities generate a fourth free position available to link ancillary ligands to yield distorted square planar (SP-4) species, which usually incorporate one or two further ligands to generate square pyramidal (SPY-5) or octahedral (OC-6) polyhedra (Scheme 3).
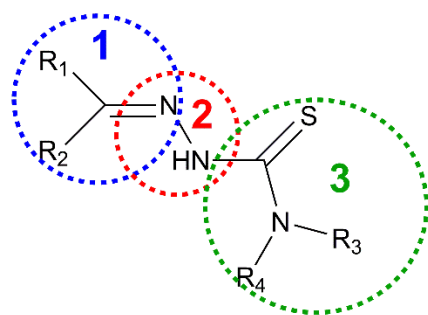
Scheme 1. Fragments in thiosemicarbazone group.
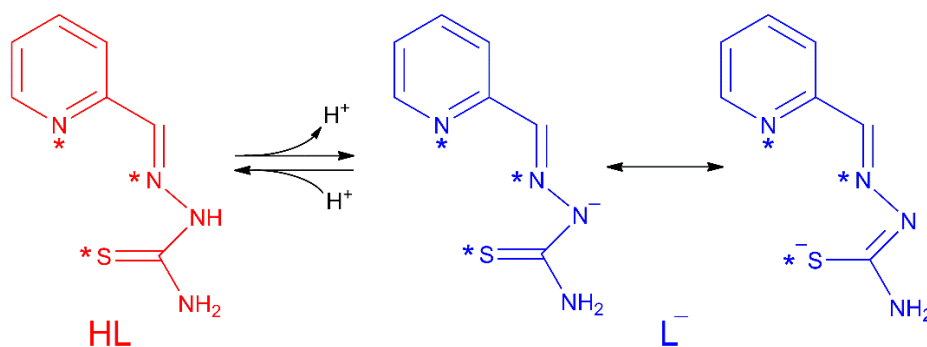
Scheme 2. Acid-base behaviour in the HL thiosemicarbazone. Asterisks (*) denote donor chelating centres.
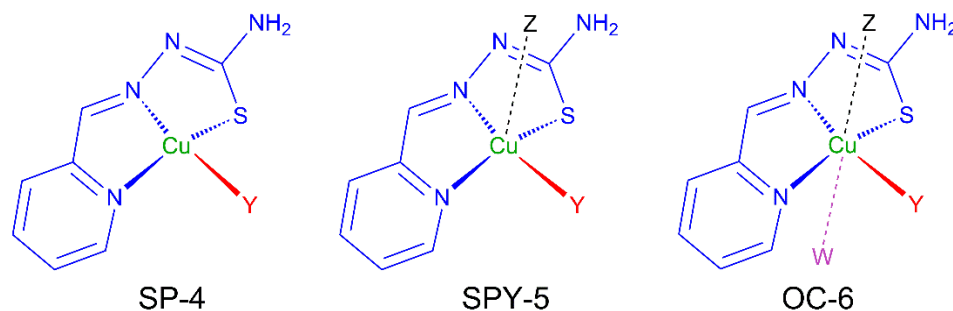
**Scheme 3.** Usual geometries for monomers containing $[CuL]^+$ fragments.

　　The presence of monodentate anionic X^- coligands gives rise to [CuLX] fragments that often arrange connecting through the apical ligand of square pyramidal polyhedra

around the Cu(II) ions to build dinuclear [{CuLX}$_2$] compounds. In this way, two types of dinuclear complexes are formed (Scheme 4):

- Compounds with the X coligand acting as a bridge between the [CuLX] entities giving rise to [Cu$_2$(μ-X)$_2$] cores (so called X-bridged systems, Scheme 4a);
- Compounds in which the S thioamide atom (S$_L$) is the bridge between monomers generating [Cu$_2$(μ-S$_L$)$_2$] fragments (S-bridged systems, Scheme 4b).
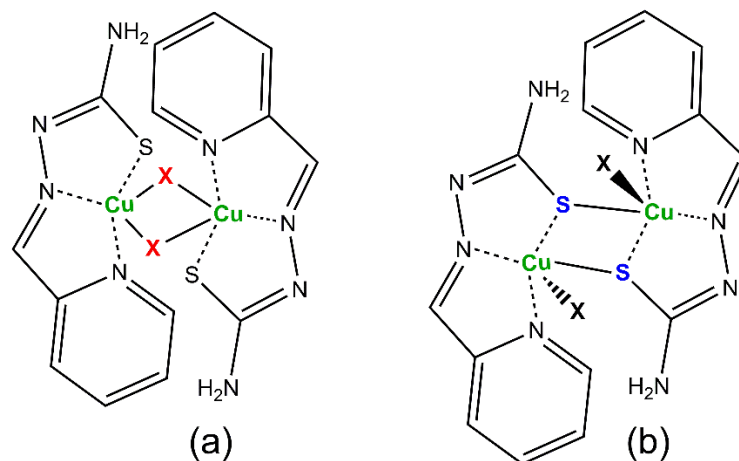
Scheme 4. Usual structures for [{CuLX}$_2$] compounds: (**a**) X-bridged, (**b**) S-bridged system.

In the case of complexes containing the L$^-$ anionic form, the presence of both kinds of dinuclear systems is majority, except for highly bulky coligands [33,34] or the [CuL$_2$] biscomplex [35]. However, the HL neutral form gives rise to X-bridged dimers and mononuclear complexes [36], a feature shared with other TSC-Cu(II) compounds [37,38]. The reluctance of the neutral HL form to be incorporated into S-bridged dimers has been interpreted as due to the lack of electron density over the S atom in the thione C=S group, enough to establish bonds perpendicular to the TSC plane with metals, in the opposite way of the sp^3 hybrid behavior of the C–S$^-$ thiolate anionic form [39]. In fact, as far as we are aware, there is only one S-bridged compound containing a neutral tridentate TSC ligand linked to Cu(II) ions, and the Cu–S distances linking neighbor monomers are as long as 2.937 Å [40]. The planarity and structural uniformity of the [CuLX] fragments in both kinds of dinuclear compounds make them suitable for molecular magnetic studies. In this regard, the S-bridged systems are particularly attractive because they allow for a more efficient control of the properties, which is easily achieved by changing the nature of X. The research carried out for years in this field has collected the results summarized in Table 1 in terms of values for the exchange coupling *J* parameter, which measures the magnetic cooperativity between the paramagnetic Cu(II) centers. The *J*-value was calculated by fitting the experimental magnetic susceptibility data to the Bleaney and Bowers's expression for copper(II) dinuclear compounds [41] derived from the Heisenberg isotropic Hamiltonian (H = −2JS$_1$S$_2$); see Equation (1). In this Equation, *N* is the Avogadro's number, *β* the Bohr magneton, *g* the Landé factor and *k* the Boltzman's constant. The table also contains the work performed on the analogous [{CuL'X}$_2$] compounds, where HL' is pyridine-2-carbaldehyde 4N-methylthiosemicarbazone (R$_1$ = py; R$_2$ = R$_4$ = H; R$_3$ = CH$_3$ in Scheme 1). Data reveal that magnetic interactions in these compounds are weak, as expected considering the long apical distance and the exchange pathway nearly perpendicular to the plane of the involved magnetic d$_{x^2-y^2}$ orbitals. Moreover, the results point to the influence of the coligands in the *J* values of S-bridged compounds, the lower electronegative X the stronger the antiferromagnetic interactions (Pauling's electronegativities O 3.44, Cl 3.16, N 3.04, Br 2.96, I 2.66). Thus, the [{CuLI}$_2$] derivative shows the largest antiferromagnetic interactions in the given series. In addition, dinuclear complexes containing the neutral HL form of the ligand seem to exhibit lower antiferromagnetic interactions than the analogous with deprotonated L$^-$ form. Magnetic interactions have been reported for other thiosemicar-

bazonecopper(II) systems and evidence a majority antiferromagnetic behavior [42–47], as those described for non-thiosemicarbazone systems [48–50].

$$\chi_m = \frac{Ng^2\beta^2}{kT}\left[\frac{2}{3 + exp\left(\frac{-2J}{kT}\right)}\right]$$ (1)

Table 1. J values (defined from a H = −2 JS$_1$S$_2$ Hamiltonian) along with some crystallographic parameters, for both S- and X-bridge dimer [{Cu(L/L')X}$_2$] systems. The first column specifies the donor atom [X] (see X in bold, in Scheme 4). The intradimeric distances are represented as Cu···Cu' (Å); X' is the apical ligand, linkages to the apical ligand are depicted as Cu···X' (Å), and bridging angles as Cu–X'···Cu' (°).

Compound [Donor Atom in the Coligand]	X'	Cu···Cu'/Cu···X' (Å)	Cu–X'···Cu' (°)	J (cm^{-1})
[{CuL(H$_2$O)}$_2$](SiF$_6$)·4H$_2$O [O] [51]	S	3.5950(4)/2.7963(6)	89.231	+4.44
[{CuL(HCOO)}$_2$] [O] [52]	S	3.503(2)/2.820(2)	86.34(5)	−2.80
[{CuL(H$_2$O)}$^{(1)}${CuL(SO$_4$)}$^{(2)}$]·H$_2$O [O] [53]	S $^{(1)}$, O $^{(2)}$	3.365(1)/2.354(3) $^{(1)}$, 2.8797(16) $^{(2)}$	80.49(4) $^{(1)}$, 101.97(13) $^{(2)}$	−3.21
[{CuL(NO$_2$)}$_2$] [O] [52]	S	3.554(1)/2.918(2)	85.5(1)	−3.40
[{CuLCl}$_2$] [Cl] [54]	S	3.486(2)/2.760(2)	87.01(4)	−3.91
[{(CuL)$_2$(dca *)}(ClO$_4$)]$_n$ [N] [55]	S	3.5953(2)/2.8383(1)	88.6(2)/85.4(2)	−3.30
[{CuL(NCS)}$_2$] [N] [56]	S	3.450(3)/2.754(5) $^{(a)}$	85.9(1) $^{(a)}$	−5.09
[{CuLBr}$_2$] [Br] [54]	S	3.474(1)/2.743(2)	87.12(5)	−5.21
[{CuLI}$_2$] [I] [57]	S	3.455(1)/2.775(1)	85.80(4)	−14.03
[{Cu(L')(NO$_3$)}$_2$] [O] [57,58]	S	3.4482(2)/2.7659(6)	85.83(2)	+6.88
[{Cu(L')(H$_2$O)}$^{(1)}${Cu(L')(SO$_4$)}$^{(2)}$]·5H$_2$O [O] [35,53]	S $^{(1)}$, S $^{(2)}$	3.435/2.8114(14) $^{(1)}$, 2.9114(13) $^{(2)}$	82.024 $^{(1)}$, 84.326 $^{(2)}$	+5.5
[{Cu(L')(H$_2$O)}$_2$][Cu(L')(H$_2$O)$_2$]$_2$(SiF$_6$)$_2$·8H$_2$O [O] [51]	S	3.351(2)/2.819(3)	81.81	+2.22
[{Cu(L')Cl}$_2$] [Cl] [51]	S	3.587(1)/2.836(1)	88.47	−4.65
[{Cu(L')Br}$_2$] [Br] [57]	S	3.577(2)/2.832(2)	88.31	−6.12
[{CuL(CH$_3$COO)}$_2$] [O] [59,60]	O	3.442(1)/2.427(2)	103.5(1)	−3.10
[{CuL(CH$_3$CH$_2$COO)}$_2$] [O] [52]	O	3.460(2)/2.387(2)	105.35(9)	−3.30
[{CuL(tfa)}$_2$] [O] [55]	O	3.689(1)/2.632(3)	105.7(1)	−3.30
[{Cu(HL)(tfa)}$_2$][tfa]$_2$ [O] [36,55]	O	3.557(4)/2.519(4)	104.8(1)	−0.20
[{Cu(HL)(SO$_4$)}$_2$] [O] [53,59]	O	3.310(1)/2.306(2)	102.7(1)	−0.75
[{Cu(L')I}$_2$] [I] [51]	I	3.836/3.1797(6)	82.56	−4.76

* dca = dicyanamide, [N(CN)$_2$]$^-$; tfa = trifluoroacetato, CF$_3$COO$^-$; HL = pyridine-2-carbaldehyde thiosemicarbazone; HL' = pyridine-2-carbaldehyde 4N-methylthiosemicarbazone. $^{(a)}$ Average values. $^{(1),(2)}$ Different fragments in non-centrosymmetric dinuclear compounds.

Taking into account the chemistry of these compounds, it is worth noting the coexistence of Cu(II) metal ions and I$^-$ ligands in the [{Cu(L/L')I}$_2$] dimers [51,57]. This behavior is relatively unusual due to the well-known trend towards the reduction to Cu(I) ions in the presence of iodide with concomitant formation of I$_2$. In fact, few TSC-Cu(II)-iodido complexes have been reported to date, and all of them contain anionic TSCs [61–71]. Regarding the particular system derived from HL, the crystal structure of the [Cu(TSC)Br$_2$]·H$_2$O has been described [72], but studies with iodide in acid medium have not been performed to date.

In order to get insight into the chemical and structural features of TSC-Cu-I compounds, here we provide a comparative study between the iodido and chlorido chemistries of thiosemicarbazonecopper complexes derived from HL both in acid and neutral media. In this way, we have synthesized and characterized the [{CuLX}$_2$] (X = Cl$^-$ (**1**), I$^-$ (**2**)), [Cu(TSC)Cl$_2$]·H$_2$O (**3**) and [{Cu(H$_2$L)I$_2$}$_2$] (**4**) compounds. Computational calculations are

performed in two ways: (i) to visualize the thermodynamic differences of the chemical behavior and (ii) to explain the magnetic properties in the [{CuLX}$_2$] (X = Cl$^-$, I$^-$) S-bridged dimers. We have found that the structural analogies in complexes containing anionic L$^-$ are lost in the acid media. The latter originates a [Cu(HL)Cl$_2$]·H$_2$O compound, while the presence of I$^-$ anions induces a reduction process leading to the formation of [{Cu(H$_2$L)I$_2$}$_2$] dinuclear Cu(I) species. Computational studies point to a larger stability of the chlorido complexes in aqueous medium. Finally, the DFT molecular-based calculations carried out to explain the magnetic behavior of [{CuLX}$_2$] (X = Cl$^-$, I$^-$) S-bridged dimers show that the choice of functionals largely influences the results. Notwithstanding, no success is found in the reproducibility of the experimental results for the iodido derivative in any of the used methods, most of which paradoxically predict ferromagnetic intramolecular interactions for this compound.

2. Results and Discussion

2.1. Synthesis of the Compounds

Syntheses of complexes **1** and **2**, with formulae [{CuLX}$_2$] (X = Cl (**1**) and I (**2**), have been published in different papers [54,57,59]. The present work describes a method for the preparation of **1** based on the use of CuCl$_2$ and aqueous medium, very slightly different to those reported in the literature. Regarding **2**, the iodide salt stabilizes de Cu(I) oxidation state due to the reducing character of I$^-$. Because of this, a new strategy must be used such as that involving the very soluble CuL(ClO$_4$) compound as a reactant, which is prepared in situ by mixing Cu(ClO$_4$)$_2$ and HL in aqueous solution. The addition of NaI or KI yields the immediate precipitation of compound **2**. Both compounds, **1** and **2**, can be obtained from aqueous solutions at pH 2–8 and even slightly outside this broad range.

Ethanolic solutions favor the attainment of solids containing non-deprotonated HL ligand due, at least in part, to the high solubility these compounds exhibit in aqueous solutions. In the case of **3**, the [Cu(HL)Cl$_2$]·H$_2$O is formed from the direct reaction of CuCl$_2$ and HL in acid HCl medium. It contains Cu(II) ions linked to a neutral HL ligand. However, the synthesis of compound **4** was carried out starting from [{CuLI}$_2$] (**2**) as a reactant and purified HI (c) as an acid. A reduction process took place yielding the [{Cu(H$_2$L)I$_2$}$_2$] compound, which contains Cu(I) ions bonded to cationic pyridinium-2-carbaldehyde thiosemicarbazone (H$_2$L$^+$) species. This result emphasizes that the HL-Cu(II) system hardly bears the incorporation of a second iodido coligand, without experiencing the reduction of the metallic center, in good agreement with previously reported studies [64].

2.2. Crystal Structure

As mentioned before, the crystal structures of compounds **1** and **2** are made up of S-bridged [{CuLX}$_2$] centrosymmetric dimers, with square-pyramidal Cu(II) ions bonded to the pyridine and azomethine nitrogen atoms and to the thioamide sulfur atom of the TSC ligand, which behaves as a NNS tridentate chelate ligand. The fourth basal plane position is occupied by an halido ligand, and the apical vertex is formed by the S thioamide atom of the neighbor [CuLX] moiety, which acts as a bridge [54,57].

The crystal structure of **3** contains monomeric [Cu(HL)Cl$_2$] entities and one crystallization water molecule per formula (Figure 1). The Cu(II) ion is coordinated to the NNS chelating set of the TSC ligand and two chlorido ligands in an square pyramid fashion, $\tau_5 = (\alpha - \beta)/60 = 0.06$ (ranging from $\tau_5 = 0$ square pyramid SPY-5 to $\tau_5 = 1$ trigonal bipyramid BPT-5 geometries) [73]. Selected distances and angles are provided in Table 2. A choice of structural parameters (i.e., bonds, angles and non-bonding contacts) allows one to identify the neutral (HL) vs. anionic (L$^-$) character of the TSC ligand [74]. These parameters are C7–S, Cu···N3, N2···C7, Cu–N2–N3, N2–N3–C7, S–C7–N3 and S–C7–N4 whose values in **3** are 1.7076(1) Å, 2.9068(3) Å, 2.3003(2) Å, 120.13(1)°, 118.20(1)°, 121.03(1)° and 121.78(1)°, respectively, which fall in the range of those expected for Cu(II) compounds containing non-deprotonated neutral TSC ligands. The lattice is stabilized with hydrogen bonds involving the hydrazine N3, thioamide N4, apical chlorido Cl2 and water O atoms

(see Supporting Information). π-π Interactions between pyridine and thioamide fragments of neighbor entities are also present and, probably, anion-π interactions with Cl···C6^i distances of 3.4576(3) Å (i = −x + 1, −y, −z+1). The closest Cu(II) ions are placed at 4.182(6) Å.
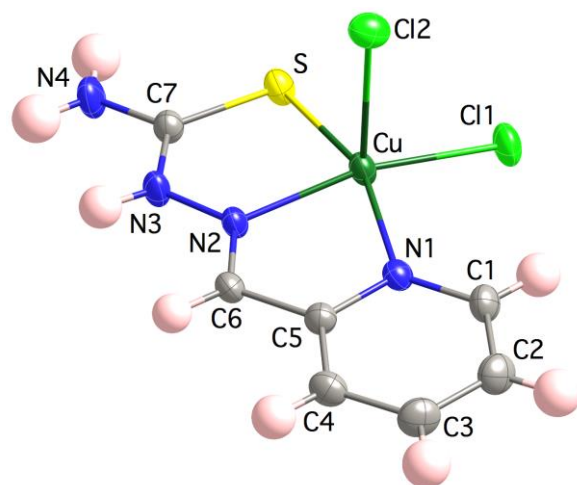
Figure 1. Crystal structure of the [Cu(HL)Cl$_2$] unit in **3**. Thermal ellipsoids are drawn at 30% probability level.

Table 2. Selected bond distances (Å) and angles (°) for compounds **3** and **4**.

| Bonds and Angles	Compound 3	Compound 4
Cu–N1	2.0429(2)	−
Cu–N2	1.9886(2)	−
Cu–S	2.3057(2)	2.293(3)
Cu–Cl1/I1	2.2465(2)	2.6754(18)
Cu–Cl2/I2	2.5896(2)	2.6154(16)
Cu–I1′	−	2.7761(17)
C6–N2	1.2698(1)	1.252(12)
C7–N3	1.3355(1)	1.331(12)
C7–N4	1.3140(1)	1.311(12)
N2–N3	1.3453(1)	1.365(10)
C7–S	1.7076(1)	1.681(9)
X1–Cu–X2	97.20(1)	117.78(6)
S–Cu–X1	95.29(1)	118.25(9)
S–Cu–X2	96.51(1)	101.95(8)
N2–Cu–N1	78.66(1)	−
N2–Cu–Cl1	162.89(1)	−
N1–Cu–S	159.44(1)	−
N2–Cu–Cl2	99.90(1)	−
Cu–N2–N3	120.13(1)	−
N2–N3–C7	118.20(1)	121.9(7)
N3–C7–N4	117.19(1)	117.4(8)
S–C7–N3	121.03(1)	120.2(7)
S–C7–N4	121.78(1)	122.4(7)

As a whole, the crystal structure of **3** strongly resembles that of the [Cu(TSC)Br$_2$]·H$_2$O derivative [72]. The structural trends exhibited by **1** and **3** in the HL-Cu(II)-Cl system, i.e., formation of [{CuLCl}$_2$] dimers, [Cu(HL)Cl$_2$] monomers and even [CuL$_2$] complexes in 1:2 metal-to-ligand ratios, are also reflected by other TSC-Cu(II)-Cl and semicarbazone systems [75].

Compound **4** is formed with dinuclear [{Cu(H$_2$L)I$_2$}$_2$] motives (Figure 2), where each of the Cu(I) ions is bonded to a terminal I$^−$ ligand, the thioamide S atom and two bridging iodido ligands that generate a [Cu$_2$(μ-I)$_2$] core. Note that the TSC ligand behaves as monodentate, stabilizing soft-to-soft Cu(I)–S bonds, in good agreement with most of the structures reported for TSC-Cu(I) species. The coordination polyhedron is clearly

tetrahedral, $\tau_4 = [360 - (\alpha + \beta)]/141 = 0.88$ ($\tau_4 = 0$ square planar SP-4 vs. $\tau_4 = 1$ tetrahedral T-4 geometries) [76]. It is worth noting that the C7–S bond length is extraordinarily similar to that in the (H_2L)Cl·H_2O compound, two molecules in the asymmetric unit with C7–S bond lengths of 1.687(6) and 1.680(6) Å [77,78], and even shorter than that in the free ligand HL·nH_2O structure, 1.698 Å [55,79–81]. The intramolecular Cu···Cu' distance is 3.662(3) Å, while the closest intermolecular Cu(I) are 7.570(2) Å away. The shortening of both, Cu–S and C7–S bond lengths in compound **4** with respect to those in compound **3** (see Table 2), despite the former containing larger Cu(I) ions, could be due to the presence of a charge transfer in **4** which is responsible for its reddish color.
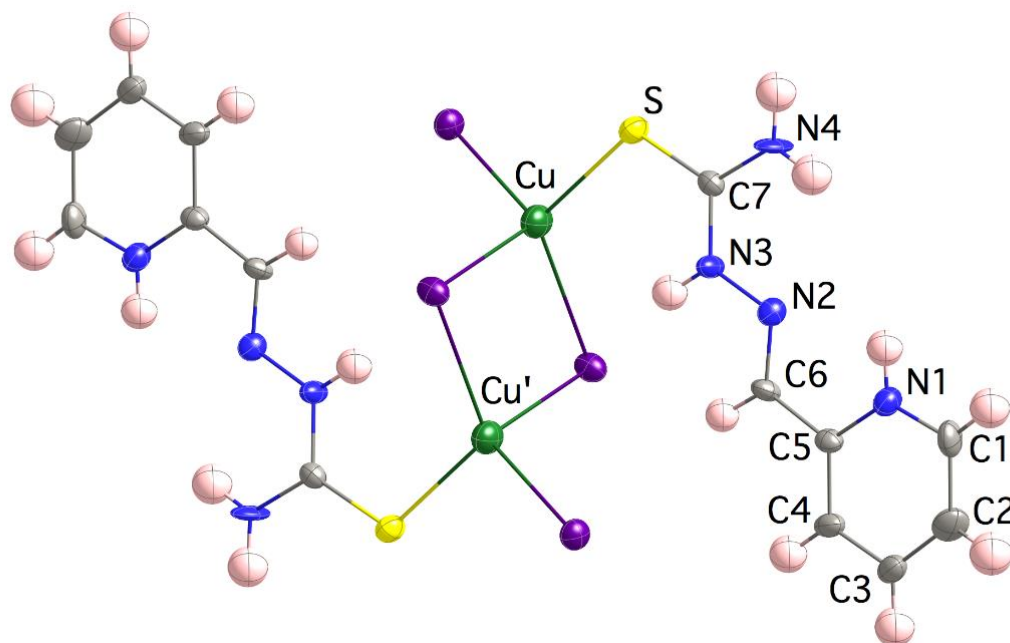

Figure 2. Crystal structure of the [{Cu(H_2L)I_2}$_2$] motives in **4**. Thermal ellipsoids are drawn at 30% probability level.

The E configuration around the C6=N2 bond is favored due to the presence of an intraligand N1–H···N2 bond. It contrasts with the original E configuration in compound **3,** as a result of the coordination to the metal ion. N1 and N2 exhibit a syn conformations with respect to the C5–C6 bond, while S and N2 are anti with respect to the C7–N3 linkage. Both conformations and the mentioned configuration exactly reproduce those of the free H_2L^+ cation in the (H_2L)Cl·H_2O compound [77]. Weak π-π interactions are established between TSC chains of neighbor dimers (minimum distances of 3.583(11) Å N3···N2^i, i = −x + 2, −y + 1, −z + 1 and 3.409(19) Å C3···C3^{ii}, ii = −x + 2, −y, −z + 1) and anion-π interactions with N1···I2^{iii} distances of 3.627(9) Å (iii = −x + 3/2, y−1/2, −z + 1/2).

As far as we are aware, the accumulation of three I$^−$ ligands around any metal center in TSC complexes only has one precedent in the analogous [Hg$_2$(HL")I_4] compound that contains Hg(II) ions linked to the benzaldehye 4N,4N-dimethylthiosemicarbazone [82] in a way identical to that in **4**.

2.3. Infrared Spectroscopy

Strong analogies are observed in the IR, the spectra of the compounds **1** and **2** (Figure 3). However, **3** and **4** are different (Figures 4 and 5). Despite the great complexity, a tentative assignment for the bands can be completed (see Figures S1.4–S1.6, Table S1.2 and text below).
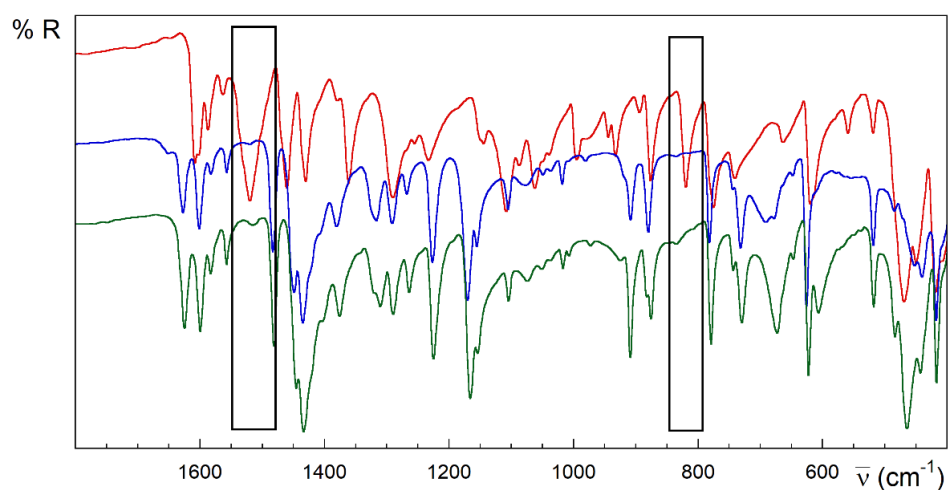
Figure 3. FTIR-ATR spectra of HL (red), *1* (blue) and *2* (green). Rectangles in black highlight the main differences between the spectra of the free ligand and [{CuLX}$_2$] complexes.
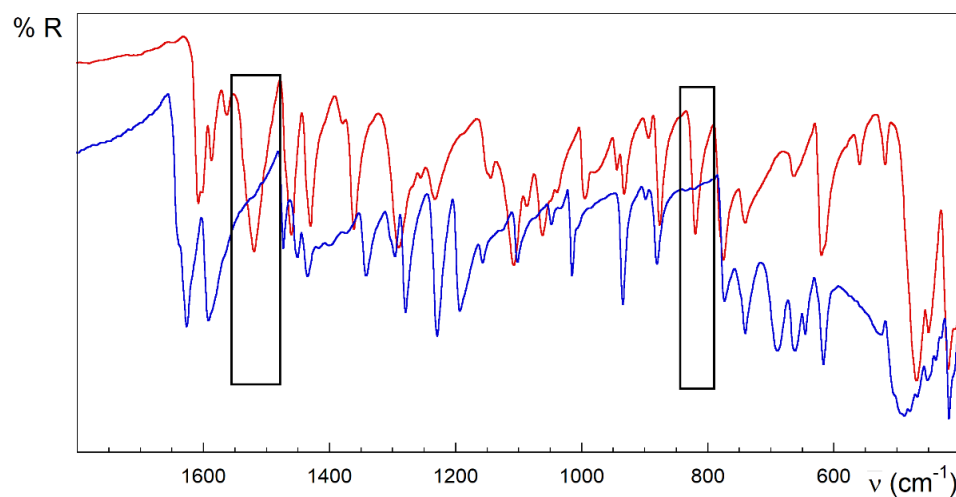
Figure 4. FTIR-ATR spectra of HL (red) and *3* (blue). Rectangles in black highlight the main differences between the spectra of the free ligand and the complex.
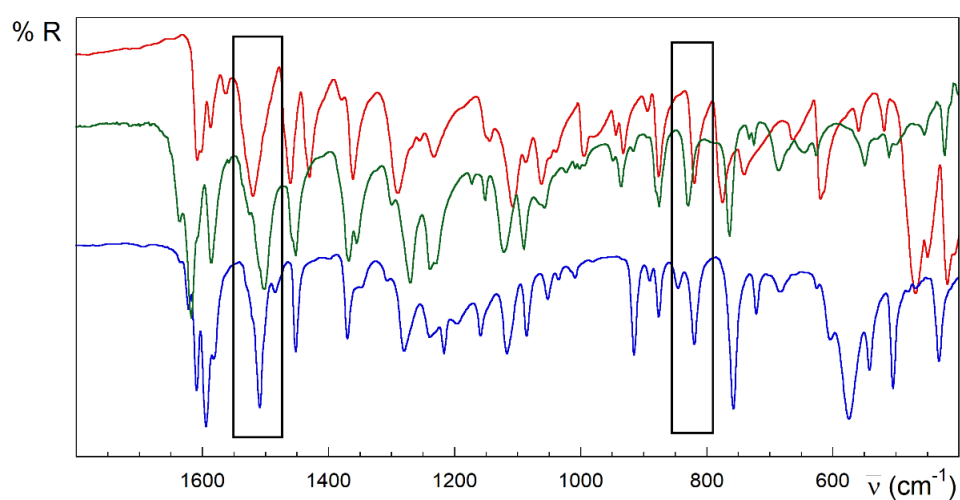
Figure 5. FTIR-ATR spectra of HL (red), (H$_2$L)Cl·H$_2$O (green) and *4* (blue). Rectangles in black show bands in the same spectral regions for the three compounds.

The bands located above 3000 cm^{-1} are attributed to the υ(OH), υ(NH), υ(NH$_2$) and υ(C=H) stretching vibrations [72,83]. A weak band observed between 3075 and 2970 cm^{-1} would correspond to the stretching ν(CH) vibration. A broad band about 2650 cm^{-1} is present in the spectrum of **3**. This band can be attributed to the ν(NH) vibration involving the strong N3–H···O^{iii} hydrogen bond (iii = $-x + 1$, $y - 1/2$, $-z + 1/2$), with N3···O distance of 2.6886(2) Å.

The strong band observed at 1608 cm^{-1} mode in the HL free ligand could be attributed to the υ(C=N) stretching modes from the pyridine and azomethine nitrogen atoms and bending vibration of the terminal amino group δ(N4–H). This band increases in energy for complexes, which could be related to the π-backdonation from the full metal orbitals to the ligand ones. In addition, there are two relevant intervals at 1595–1510 and 1455–1430 cm^{-1}, known as tioamide I and II bands [51], which are attributed to mixtures of the stretching and deformation modes of the C–S, C–N and N–H bonds in the thioamide group. The very strong band at 1520 cm^{-1} in the free HL ligand completely vanishes on complexation in compounds with anionic (L$^-$) or neutral (HL) ligand, including **1**, **2** and **3** (see the rectangles in Figures 3 and 4). However, it remains slightly shifted to 1509 cm^{-1} in compound **4**, keeping the intensity (Figure 5). This band could be attributed to vibration modes rich in hydrazine δ(N3–H) contribution. The lack of this band in compound **3** could be due to the influence of the conformation in this absorption. In this sense, note the anti-conformation exhibited by S and N2 with respect to the N3–C7 bond in free HL and free or coordinated cationic H$_2$L+ forms, which contrasts with the syn conformation in metal complexes where the TSC acts as a tridentate ligand.

It must be pointed out that bands in the 1640−1580 cm^{-1} region are more intense than those at 1490−1400 cm^{-1} for compounds with the neutral thiosemicarbazone ligand, as **3**. The opposite tendency is observed for copper(II) complexes containing anionic deprotonated TSC, such as **1** and **2** (see regions A and B in Figure S1.7). This ratio of intensities is useful to distinguish the presence of neutral (HL) vs. anionic (L$^-$) forms in the metal complexes.

Multiple bands appear around 1380–1000 cm^{-1}, which are attributed to thioamide III [84]. The absorption at 820 cm^{-1} in HL is assigned to the thioamide IV mode, with high υ(C=S) contribution. This band disappears in the compounds **1–3** whose TSC ligand behaves like a tridentate ligand (NNS system) (rectangles in Figures 3 and 4). This disappearance has been related to the loss of thione C=S character in TSC upon coordination of the metal ion. On the contrary, complex **4** preserves this band without losing intensity, in good agreement with the results with TSC monodentate ligands linked to Cu(I) ions through the thioamide S donor atom [85]. Notwithstanding the traditionally assumed interplay between this band and the double-bond character of the C7–S linkage, the presence of this feature could be also related to the influence of the aforementioned anti-conformation around the N3–C7 bond on the coupled C7–S vibration modes. This feature is common to free HL, cationic H$_2$L$^+$ species and some complexes with Cu(I) ions where HL behaves as a monodentate S-donor ligand [86,87]. Several bands in the 780–720, 685–615, 780–720 and 435–415 cm^{-1} ranges are assigned to different in-plane and out-of-plane vibrational modes of the pyridine ring [88].

2.4. Electronic Paramagnetic Resonance

As it has been previously reported, [{CuLX}$_2$] (X = Cl$^-$ and I$^-$) exhibit rhombic (g$_1$ = 2.183, g$_2$ = 2.053 and g$_3$ = 2.033) and isotropic (g = 2.074) signals, respectively [54,57].

The EPR spectrum of compound **3** shows an axial signal with g$_{\parallel}$ = 2.209 and g$_{\perp}$ = 2.050 [72]. The spectra of **1** and **3** are characteristic of d$_{x2-y2}$ ground states, similar to those arisen from Cu(II) centers in square-based pyramidal environments. The spectroscopic and magnetic behaviors of these chlorido species are parallel to those in the bromido ones [54,72]. On the other hand, the isotropic curve in **2** is compatible with several interpretations, such as dynamic Jahn–Teller effects, dipolar interactions and magnetic exchange influences. In contrast to the others, compound **4** does not show any significant EPR signal, which is

consistent with the presence of diamagnetic Cu(I) species, except for a very small amount of impurities of the [{CuLI}$_2$] reactant used as starting material (Figure S1.9d).

2.5. Computational Studies

2.5.1. Thermodynamics

In order to consider the reasons to explain the differences in the behavior of the iodide and chloride anions, the thermodynamics of the reactions of the different possibilities of the copper complexes has been theoretically calculated for both the neutral (HL) and the anionic (deprotonated) (L$^-$) ligands. In the case of the complexes with the HL neutral ligand, the formation of the chlorido derivatives seems to be thermodynamically more favored than the formation of the iodido derivatives (see Table 3). Geometrically, the substitution of aqua ligands with chlorido or iodido ligands mostly lead to pseudooctahedal structures or square pyramids (derived from the octahedral geometry moving away one of the ligands; see Figures S2.1 and S2.2).

Table 3. Free energy of the reactions for the successive substitution of aqua ligands with iodide or chloride in [Cu(HL)(OH$_2$)$_3$]$^{2+}$.

Isomer	ΔG (kcal/mol)
[Cu(HL)(OH$_2$)$_3$]$^{2+}$ + Cl$^-$ → [Cu(HL)Cl(OH$_2$)$_2$]$^+$ + H$_2$O	
[Cu(HL)Cl(OH$_2$)$_2$]$^+$ trans	−29.99
[Cu(HL)Cl(OH$_2$)$_2$]$^+$ cis	−34.39
[Cu(HL)(OH$_2$)$_3$]$^{2+}$ + 2Cl$^-$ → [Cu(HL)Cl$_2$(OH$_2$)] + 2H$_2$O	
[Cu(HL)Cl$_2$(OH$_2$)] trans	−54.46
[Cu(HL)Cl$_2$(OH$_2$)] cis1	−43.81
[Cu(HL)Cl$_2$(OH$_2$)] cis2	−43.60
[Cu(HL)(OH$_2$)$_3$]$^{2+}$ + 3Cl$^-$ → [Cu(HL)Cl$_3$]$^-$ + 3H$_2$O	
[Cu(HL)Cl$_3$]$^-$	−56.37
[Cu(HL)(OH$_2$)$_3$]$^{2+}$ + I$^-$ → [Cu(HL)I(OH$_2$)$_2$]$^+$ + H$_2$O	
[Cu(HL)I(OH$_2$)$_2$]$^+$ cis1	−0.91
[Cu(HL)I(OH$_2$)$_2$]$^+$ trans	−2.06
[Cu(HL)I(OH$_2$)$_2$]$^+$ cis2	−1.17
[Cu(HL)(OH$_2$)$_3$]$^{2+}$ + 2I$^-$ → [Cu(HL)I$_2$(OH$_2$)] + 2H$_2$O	
[Cu(HL)I$_2$(OH$_2$)] trans	−2.02
[Cu(HL)I$_2$(OH$_2$)] cis1	−1.15
[Cu(HL)I$_2$(OH$_2$)] cis2	−1.75
[Cu(HL)(OH$_2$)$_3$]$^{2+}$ + 3I$^-$ → [Cu(HL)I$_3$]$^-$ + 3H$_2$O	
[Cu(HL)I$_3$]$^-$	−1.01

ΔG Gibbs free energy. The labels cis and trans refer to the relative position of the aqua ligand that was substituted in the complex [Cu(HL)(OH$_2$)$_3$]$^{2+}$ before the optimization of the geometry.

Depending on the pH of the reaction, the ligand thiosemicarbazone can undergo deprotonation. In the case of the deprotonated ligand, the successive substitution of aqua ligands with chloride or iodide can be simulated as well. The structures obtained for the different possibilities of substitution are collected in Figures S2.3 and S2.4. As in the case of the non-deprotonated thiosemicarbazone ligand, the formation of the chlorido complexes seems to be favored over the formation of the iodido complexes (see Table 4). In the case of the iodido complexes, only the formation of the square pyramid obtained through the substitution of one aqua ligand seems to be slightly favored. The geometry of the complexes obtained through substitution of one or two aqua ligands with chlorido ligands

are square pyramids through decoordination of one water molecule. In the case of the total substitution of the aqua ligands, it forms a distorted octahedral structure. Interestingly, the iodido derivatives keep the water coordinated to the copper.

Table 4. Free energy of the reactions for the successive substitution of aqua ligands with iodide or chloride in $[CuL(OH_2)_3]^{2+}$.

| Isomer	ΔG (kcal/mol)
$[CuL(OH_2)_3]^+ + Cl^- \rightarrow [CuLCl(OH_2)_2] + H_2O$	
$[CuLCl(OH_2)_2]$ cis1	−30.59
$[CuLCl(OH_2)_2]$ trans	−28.58
$[CuLCl(OH_2)_2]$ cis2	−30.52
$[CuL(OH_2)_3]^+ + 2Cl^- \rightarrow [CuLCl_2(OH_2)]^- + 2H_2O$	
$[CuLCl_2(OH_2)]^-$ trans	−47.96
$[CuLCl_2(OH_2)]^-$ cis1	−39.35
$[CuLCl_2(OH_2)]^-$ cis2	−39.48
$[CuL(OH_2)_3]^+ + 3Cl^- \rightarrow [CuLCl_3]^{2-} + 3H_2O$	
$[CuLCl_3]^-$	−35.33
$[CuL(OH_2)_3]^+ + I^- \rightarrow [CuLI(OH_2)_2] + H_2O$	
$[CuLI(OH_2)_2]$ cis1	−0.87
$[CuLI(OH_2)_2]$ trans	1.67
$[CuLI(OH_2)_2]$ cis2	−0.54
$[CuL(OH_2)_3]^+ + 2I^- \rightarrow [CuLI_2(OH_2)]^- + 2H_2O$	
$[CuLI_2(OH_2)]^-$ trans	0.30
$[CuLI_2(OH_2)]^-$ cis1	1.61
$[CuLI_2(OH_2)]^-$ cis2	0.74
$[CuL(OH_2)_3]^+ + 3I^- \rightarrow [CuLI_3]^{2-} + 3H_2O$	
$[CuLI_3]^-$	3.33

ΔG Gibbs free energy. The labels cis and trans refer to the relative position of the aqua ligand that was substituted in the complex $[CuL(OH_2)_3]^+$ before the optimization of the geometry.

2.5.2. Magnetic Properties

In order to clarify the underlying reasons for the magnetic properties in compounds **1** and **2**, DFT (B3LYP functional) calculations by using the experimental atomic coordinates of the dinuclear structural unit of the complex were performed. These studies were extended to other compounds given in Table 1, which contain neutral HL/HL′ or deprotonated L^-/L'^- forms of the TSC ligands. In the following discussion, the values given for the magnetic exchange *J* parameter are those derived from the Heisenberg isotropic spin Hamiltonian H = $-2JS_1S_2$, see Scheme 5. Therein, $2J = E_{S=0} - E_{S=1} = E$, where $E_{S=0}$ is calculated with the broken symmetry approach (BS); see details below and in Materials and Methods.

Taking into account that compound **2** exhibits the largest antiferromagnetic interactions in the series given in Table 1, it was our first choice to perform DFT calculations. Surprisingly, the results of the theoretical calculations predicted intradimer ferromagnetic interactions for **2** (Table 5). Two main features differentiate **2** from other compounds where the same methodological approach has yielded excellent results [89]: (i) the presence of heavy iodido ligands linked to Cu(II) ions and (ii) the connectivity of the [CuLI] monomers through

S-bridging centers to form S-bridged dimers containing $[Cu_2(\mu\text{-}S_L)_2]$ cores (Figure 6a). Aiming to check the influence of the iodido coligands, the $[\{CuL(HCOO)\}_2]$ compound was assayed, reviewing an S-bridged centrosymmetric dimer with the same TSC and formato HCOO$^-$ coligands bonded to the Cu(II) ions through light O atoms (Figure 6b). Again, a ferromagnetic result was obtained, opposite to the antiferromagnetic experimental behavior.
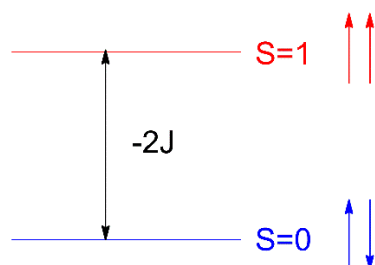
Scheme 5. Energy levels for a dinuclear system of Cu(II) ions.
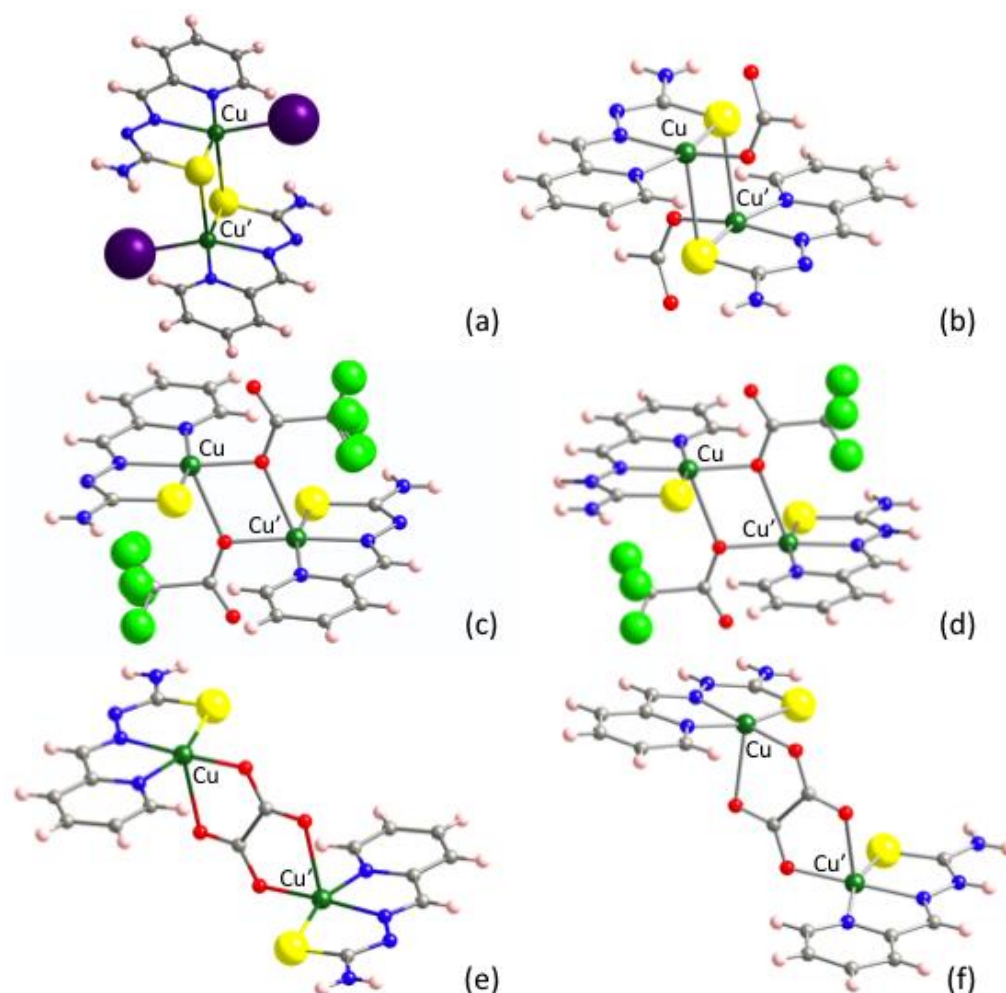
Figure 6. Molecular structures of the here explored complexes. (**a**) $[\{CuLI\}_2]$ (**2**), (**b**) $[\{CuL(HCOO)\}_2]$, (**c**) $[\{CuL(tfa)\}_2]$, (**d**) $[\{Cu(HL)(tfa)\}_2]^{2+}$ dimers in $[\{Cu(HL)(tfa)\}_2][tfa]$, (**e**) $[\{CuL\}_2(ox)]$ in $[\{CuL\}_2(ox)]\cdot2H_2O$ and (**f**) $[\{Cu(HL)\}_2(ox)]^{2+}$ dinuclear entities in $[\{Cu(HL)\}_2(ox)](NO_3)_2$.

Considering that the disagreements between experimental and calculated magnetic interactions could be due to the influence of the S-bridging centers, the $[\{CuL(tfa)\}_2]$ dinuclear complex was analyzed, reviewing an antiferromagnetic X-bridged dimer where trifluoroacetato coligands depict a $[Cu_2(\mu\text{-}O)_2]$ bridging fragment (Figure 6c). The output was also ferromagnetic.

At this stage, when none of the calculations reproduced the sign of the experimental magnetic interactions, we checked if the neutral (HL) or anionic (L^-) form of the TSC ligand could play any role. Note that the thione (C=S) contribution is greater in HL, while a (C–S^-) thiolate-like character dominates in (L^-). A structurally very similar compound to [{CuL(tfa)}$_2$] containing neutral HL ligand is the antiferromagnetic [{Cu(HL)(tfa)}$_2$][tfa]$_2$ derivative (Figure 6d). Once again, the calculations performed on the [{Cu(HL)(tfa)}$_2$]$^{2+}$ cationic dinuclear entity resulted in ferromagnetism. However, the magnitude of the ferromagnetic interactions seemed to follow the experimental trend that suggests a neutral HL form leads to lower antiferromagnetic interactions (Table 5). Finally, we tried to reproduce this trend by comparing the calculations on [{CuL}$_2$(ox)]·2H$_2$O and [{Cu(HL)}$_2$(ox)](NO$_3$)$_2$ compounds, whose dinuclear entities contain L^- and HL forms of the ligand, respectively (Figure 6e,f). The latter is the only ferromagnetic compound reported in Table 6. As can be seen, despite the disagreement in the sign of the magnetic interaction in [{CuL}$_2$(ox)]·2H$_2$O, the influence of the ligand seems to be supported too.

These results prompted us to take into account a possible influence of the intermolecular interactions in **1** and **2**, as it had been proposed for other TSC-Cu(II) dinuclear compounds showing the same contradiction between the DFT results and the magnetic measurements [90]. The DFT calculations were performed following an analogous methodology (for details, see DFT Methodology and Computational Details) and led to the following parameters: J = 3.8 cm^{-1} for complex **1** and J = 2.5 cm^{-1} for **2**. Thus, contrary to our antiferromagnetic experimental results, these calculations again indicated that the magnetic interactions inside the dinuclear complex would be ferromagnetic. Taking into account these facts, we selected three additional dinuclear models extracted from the crystal structure of complex [{CuLBr}$_2$], arbitrarily chosen to analyze independently each interdinuclear interaction. Only one fragment of each dinuclear complex was considered in all three cases. Model 1 considers the interaction (J_1) through the (N···H−N) hydrogen bonds (see Figure S2.5a in Supporting Information). Model 2 considers the stacking between two [CuLBr] units (J_2, Figure S2.5b). Model 3 analyzes S···H–C interactions (J_3, Figure S2.5c). In all three cases the values obtained are antiferromagnetic: J_1 = −0.9 cm^{-1}, J_2 = −0.85 cm^{-1} and J_3 = −0.25 cm^{-1}. The calculated dinuclear interaction for [{CuLBr}$_2$] was also ferromagectic (J = 4.6 cm^{-1}). However, the simulation of these ferromagnetic intramolecular interactions and antiferromagnetic intermolecular interactions in the [{CuLBr}$_2$] compound yielded unsuccessful results with respect to the χ vs. T curve (see Figure S2.6). Because of this, it is difficult to explain the whole antiferromagnetic behavior experimentally observed taking into account the theoretically predicted weak magnitude of them. Note that even antiferromagnetic chains gave better results than any of the scenarios theoretically considered (Figure S2.6a vs. Figure S2.6f).

Table 5. Experimental (J_{exp}) and calculated (J_{calc}) *J*-values, H = −2JS$_1$S$_2$, using the Broken Symmetry Approach of the Exchange Coupling Constants.

Compound	Reference	J_{calc} (cm^{-1})	J_{exp} (cm^{-1})
[{CuLI}$_2$] **(2)**	-	1.50	−14.03
[{CuL(HCOO)}$_2$]	[52]	1.50	−2.8
[{CuL(tfa)}$_2$]	[55]	1.26	−3.3
[{Cu(HL)(tfa)}$_2$][tfa]$_2$	[55]	1.56	−0.3
[{CuL}$_2$(ox)]·2H$_2$O	[91]	0.03	−4.30
[{Cu(HL)}$_2$(ox)](NO$_3$)$_2$	[91]	3.30	5.37

In order to examine the influence of the basis set used in the calculation of the magnetic interaction in complexes **1** and **2** per their interplay with the energy gaps between them (ΔE = E$_{S=0}$ − E$_{S=1}$), we calculated exchange coupling constants *J* based on *J* = (E$_{S=0}$ − E$_{S=1}$) [92] that derived from the spin Hamiltonian H = −JS$_1$S$_2$. Considering that in the present work

the spin Hamiltonian is defined H = $-2JS_1S_2$, the actual values of the estimated J collected in Table 6 are divided by two. The best correlation of the calculated values with the experimental measurements is given with the set of basis (a) in the chlorido complex. Nevertheless, the best correlation in both complexes (chlorido and iodido) is found when the (f) basis set is used, reproducing an antiferromagnetic behavior that is more intense for the iodido complex but with overestimated values.

Table 6. Calculated values using the Broken Symmetry Approach of the Exchange Coupling Constants for complexes **1** and **2**. In the second column, the J values are given according to H = $-2JS_1S_2$.

Compound	Basis Set *	ΔE (cm^{-1})	J (cm^{-1})
1	a	−10.36	−5.18
	b	−1.22	−0.61
	c	7.20	3.60
	d	6.76	3.38
	e	−77.61	−38.80
	f	−28.88	−14.44
2	a	3.38	1.69
	b	2.55	1.27
	c	4.61	2.30
	f	−72.76	−36.38

* (a) SDD for Cu and 6-31G(d,p) for the other elements. (b) SDD for Cu, S and the halogen atoms, and 6-31G(d,p) H, C and N. (c) TZVP for Cu and 6-31G(d,p) for the other elements. (d) TZVP for Cu and SV for the other elements. (e) LANL2DZ for Cu and 6-31G(d,p) for the other elements. (f) LANL2DZ for Cu and SV for the other elements.

The disagreement and variability in the results directed us to use other alternative approaches using techniques designed for solids. SIESTA and VASP [93–95] are efficient codes to perform DFT calculations on periodic systems, but they can also be used to study the electronic structure of isolated molecules through periodically repeating images of the molecule with enough vacuum between them. SIESTA uses localized basis sets and VASP projector-augmented waves to expand the electronic wave functions, and in both calculations, we have used the GGA (Generalized Gradient Approximation) in the PBE parametrization [96] to treat the exchange–correlation energy. Starting from the experimental structure, the atomic positions were relaxed for the ferromagnetic and antiferromagnetic configurations. The evaluation of the magnetic coupling presents opposite signs with both codes. According to SIESTA, the [{CuLCl}$_2$] isolated dimer is ferromagnetic with a magnetic coupling of J = 1.97 cm^{-1}, whereas the coupling obtained using VASP is antiferromagnetic, J = −1.70 cm^{-1}. In the case of the [{CuLI}$_2$] dimer, results obtained with SIESTA (VASP) indicate an antiferromagnetic (ferromagnetic) ground state with J = −0.53 cm^{-1} (J = 0.24 cm^{-1}).

Additional relaxations from several starting structures of compound *1* were performed using SIESTA. The monomers were placed at different distances from each other, and a complete minimization of the atomic positions was performed for each configuration. Results reveal the high complexity of the energy landscape even for a single dimer. It is remarkable that the relaxations evolved to different (local) minima, with the structure with the minimum energy being an antiferromagnetic configuration (J = −1.53 cm^{-1}). The energy of this structure is ~33 meV lower than the energy of the relaxation from the experimental positions.

We have also performed a Mulliken population analysis with SIESTA in order to study the local magnetic moment of each atom. Each of the monomers of the dimer has an excess/defect of electronic charge equal to −1/+1 e$^-$. The results of Table 7 show that the magnetic moment is not exclusively localized in the Cu atoms, with the contributions of the S, N and Cl ions being relevant. According to these results, the delocalization of the magnetic moment could play a relevant role to stabilize the magnetic configurations, opening new perspectives to study this family of complexes.

Table 7. Magnetic moments of the different atoms of each monomer of the [{CuLCl}$_2$] dimer in **1**, obtained from Mulliken populations.

Atoms	Magnetic Moment (μ_B)
C	0.000
H	0.018
N	0.212
S	0.214
Cl	0.154
Cu	0.402
Total	1.000

In summary, the apparent simplicity of performing DFT calculations on the [{CuLXl}$_2$ magnetic system turns into a difficult task due to the overestimation of the ferromagnetic contribution as opposed to the antiferromagnetic behavior experimentally detected in these complexes. The results are very sensitive to the structure and relative orientation of the two monomers. The disagreement is especially astonishing for compound **4**, which exhibits the most intense antiferromagnetic interactions described for these derivatives (see Table 1). Disagreements between the experimental magnetic parameters and those obtained with DFT calculations have been reported before for dinuclear Cu(II) compounds [97,98]. This fact suggests the need to address the problem through another methodological approach.

3. Materials and Methods

3.1. Materials

$CuCl_2$, $Cu(ClO_4)_2 \cdot 6H_2O$, NaOH, NaI, ethyl alcohol, chlorohydric acid (HCl), hydroiodic acid (HI), acetone, water and ether were purchased from commercial sources and used as received. HL was synthesized according to previously reported methods [99]. Although the syntheses of **1**, **2** and **3** have been previously reported [54,57,72], the present manuscript provides alternative methods that improve the yield and/or purity of the compounds.

3.2. Preparation of the Compounds

3.2.1. Compound **1** [{CuLCl}$_2$]

Solid HL (0.180 g, 1 mmol) was added over a solution of $CuCl_2$ (0.134 g, 1 mmol) in 15 mL of distilled water. The reaction mixture was stirred for 1 h. The pH of the solution was adjusted to 4.5 with addition of a NaOH (1M) solution. After 2 h with continuous stirring, the olive-green precipitate was filtered off, washed with three fractions of water, acetone and ether and dried over vacuum. (Yield 0.25 g, 90%). Anal. Calc. for $C_7H_7ClCuN_4S \cdot 1/3H_2O$ (284.23 g mol^{-1}): C, 29.6; H, 2.7; N, 19.7; S, 11.3%. Found: C, 29.6; H, 2.6; N, 19.4; S, 11.6%. Note that a small amount of water is included in the formula of *1* to fit the analysis. ESI$^+$ mass spectrometry (m/z): 240.99 [CuL]$^+$, 319.98 [CuL(DMSO]$^+$ and 520.90 [Cu$_2$L$_2$Cl]$^+$.

3.2.2. Compound **2** [{CuLI}$_2$]

$Cu(ClO_4)_2 \cdot 6H_2O$ (0.743 g, 2 mmol) were dissolved in 30 mL of distilled water, and HL ligand (0.364 g, 2 mmol) was added as a solid. The mixture is stirred for 1 h, and, then, the mint-green suspension is filtered with gravity. Afterwards, a solution of NaI (1.796 g, 12 mmol) was slowly added through an addition funnel while stirring. The pH of the moss-green solution was adjusted to 4.5 with drops of a NaOH (1M) solution. A suspension was formed and stirred for 2 h. The olive-green solid obtained is washed with three fractions of water, acetone and ether and dried over vacuum. (Yield 0.29 g, 78%). Anal. Calc. for $C_7H_7CuIN_4S$ (369.67 g mol^{-1}): C, 22.7; H, 1.9; N, 15.2; S, 8.7%. Found: C, 21.7; H, 1.8; N, 14.9; S, 8.3%. ESI$^+$ mass spectrometry (m/z): 240.98 [CuL]$^+$, 319.98 [CuL(DMSO]$^+$ and 612.84 [Cu$_2$L$_2$I]$^+$.

3.2.3. Compound **3** [Cu(HL)Cl$_2$].H$_2$O

An amount of CuCl$_2$ (0.133 g, 1 mmol) was dissolved in 20 mL of ethanol, and solid HL (0.180 g, 1 mmol) was added. The solution was acidified with drops of diluted HCl (3.5 mL, 1 mmol), and the mixture was kept with stirring for 2 h. The resulting solution was filtered off, washed with three fractions of acetone and ether and dried over vacuum. Eventually, a green precipitate was obtained. (Yield 0.28 g, 84%). Anal. Calc. for C$_7$H$_{10}$CuCl$_2$N$_4$OS (332.70 g mol^{-1}): C, 25.3; H, 3.0; N, 16.8; S, 9.6%. Found: C, 25.3; H, 3.0; N, 17.0; S, 9.2%. ESI$^+$ mass spectrometry (m/z): 241.97 [CuL]$^+$, 319.98 [CuL(DMSO)]$^+$ and 520.90 [Cu$_2$L$_2$Cl]$^+$. Recrystallization of the powder (0.02 g) was performed by using a mixture of solvents (methanol/acetonitrile, 1:1) previously acidified with 2 drops of HCl (c). Finally, 24 h later, moss green crystals were collected.

3.2.4. Compound **4** [Cu$_2$(H$_2$L)I$_4$]

The synthesis of this compound was carried out through the use of [{CuLI}$_2$] (0.185 g, 0.25 mmol), which was also prepared in our laboratory, and purified HI (9.3 mL, 0.5 mmol). Purification of HI was performed removing the plentiful I$_2$ impurities through extraction with CCl$_4$ and, in a second step, with ethyl ether. The precursor was dissolved in 20 mL of ethanol, and hydroiodic acid was added dropwise. The reaction was maintained under stirring for 2 h. Afterwards, the orange solid was filtered, washed three times with acetone and ether and dried over vacuum. (Yield 0.08 g, 15%). Anal. Calc. for C$_7$H$_9$CuI$_2$N$_4$S (499.23 g mol^{-1}): C, 16.9; H, 1.8; N, 11.2; S, 6.5%. Found: C, 17.1; H, 1.8; N, 11.7; S, 5.8%. ESI$^+$ mass spectrometry (*m/z*): 240.99 [CuL]$^+$, 319.98 [CuL(DMSO)]$^+$ and 610.84 [Cu$_2$L$_2$I]$^+$. The major amorphous powder contains small amounts of crystalline impurities of **2** and an unknown compound, together with crystalline **4** itself (see Figure S1.10). Crystals suitable for X-ray analysis were collected after the assay carried out by suspending [{CuLI}$_2$] (0.056 g, 0.08 mmol) in ethanol (20 mL). Then purified HI was added (1 mL), and the mixture was heated. The former green color turned into orange in 3 min, but the reaction was kept with heating with an additional 20 min. An orange solid (0.045 g) was filtered off. This solid was recrystallized in acetone. Due to the low solubility, the solution was heated, and a small amount of acetonitrile was added. After filtering off, the solution was kept in air for several days to dry. Two kinds of crystals were collected: green ones corresponding to compound **2** and orange ones of **4**.

3.3. Physical Measurements

Measurements of pH were carried out using a Crison micro-pH 2002 equipped with a Crison 5204 electrode. Elemental microanalyses were collected using the Thermo Scientific^{TM} Model Flash 2000 CHNS/O Analyzers. ESI$^+$ measurements were carried out on DMSO solutions of the samples with a Bruker Esquire 3000 Plus LC-MS 6545 Q-TOF Agilent instrument, using as mobile phase a water–methanol (70:30, *v/v*) mixture acidified with formic acid (0.1%), pH $\approx$ 3. IR spectra were performed with a Jasco FT-IR 4200 Fourier Transform Spectrophotometer at 4 cm^{-1} resolution, 64 scans, in the 4000–400 cm^{-1} (mid-infrared) spectral range. The equipment is provided with an attenuated total reflectance accessory, ATR PRO ONE Single reflection, equipped with a small PKS-DIF diamond crystal. X-band EPR spectra were recorded on a Bruker EMX spectrometer (9–10 GHz), equipped with a Bruker ER036TM NMR reference gaussmeter and an Agilent 53150A microwave frequency counter to fit the magnetic field and the frequency inside the cavity. All measurements were performed on powdered samples and at room temperature. The simulations of the EPR spectra were performed using the WinEPR-SimFonia version 1.25 software [100].

3.4. X-ray Crystallographic Studies

Crystal data collections were performed on a STOE StadiVari Pilatus-100 K single crystal diffractometer (multilayer monochromated Mo Kα radiation, λ= 0.71073 Å). Data frames were processed using the X-Area software package [101]. Direct methods (SIR97 [102])

were employed to solve the structures and then refined using the SHELXL-2018 [103] computer program within WINGX [104]. CCDC 2221165-2221166 contain the supplementary crystallographic data for compounds **3** and **4**.

Crystal data for compound *3*: $C_7H_{10}Cl_2CuN_4OS$ (M = 332.69 g/mol), monoclinic, space group $P2_1/c$ (no. 14), a = 8.5028(7) Å, b = 9.6046(7) Å, c = 14.8466(13) Å, β = 99.881(7)º, V = 1194.48(17) Å^3, Z = 4, T = 293(2) K, μ(MoK$_\alpha$) = 2.433 mm^{-1}, ρ$_{calc}$ = 1.85 g/cm^3, 13,091 reflections measured (4.862º ≤ 2θ ≤ 60º), 13,091 unique (twinned sample) which were used in all calculations. The final R1 was 0.067 (I > 2σ(I)), and wR2 was 0.1901 (all data).

Crystal data for compound *4*: $C_{14}H_{18}Cu_2I_4N_8S_2$ (M = 997.16 g/mol), monoclinic, space group $P2_1/n$ (no. 14), a = 9.570(2) Å, b = 12.589(2) Å, c = 10.821(3) Å, β = 95.48(2)º, V = 1297.7(5) Å^3, Z = 2, T = 293(2) K, μ(MoK$_\alpha$) = 6.577 mm^{-1}, ρ$_{calc}$ = 2.552 g/cm^3, 10,825 reflections measured (4.976º ≤ 2θ ≤ 55º), 2974 unique (R$_{int}$ = 0.1121, R$_{sigma}$ = 0.1662) which were used in all calculations. The final R1 was 0.05 (I > 2σ(I)), and wR2 was 0.0787 (all data).

3.5. Theoretical Calculations

DFT calculations in the Thermodynamics subsection were performed using Becke's three-parameter B3LYP exchange–correlation functional [105,106] implemented in ORCA 5.0.3 [107,108]. The basis sets used to define the atoms were def2-SVP [109] along with the auxiliary basis set def2/J [110] for all the elements. The empirical dispersion correction was taken into account using Grimme's dispersion with Becke–Johnson damping, D3BJ. The solvent (water) effects were considered within the self-consistent reaction field (SCRF) theory using the solvation model SMD of Trulhar et al. [111]. The optimized structures are available in the Supporting Information as xyz files.

The single-point quantum-chemical calculations of the complexes under study in the experimental geometries have been performed to calculate the exchange coupling constants in transition metal complexes, as was described in previous papers [92,112,113]. The exchange coupling constants are introduced with a phenomenological Heisenberg Hamiltonian H = $-2J$S$_i$·S$_j$ (where i and j refer to the different paramagnetic centers) to describe the interactions between the two paramagnetic transition metals present in the dinuclear complex. The hybrid B3LYP functional [105,106] has been used in all calculations as implemented in Gaussian03 [114] and Gaussian09 [115] packages, mixing the exact Hartree–Fock-type exchange with Becke's expression for the exchange functional [116] and that proposed by Lee–Yang–Parr for the correlation contribution [106]. Such functional provides calculated *J* values in excellent agreement with the experimental values [112,117,118]. Basis sets proposed by Schaefer et al. have been employed throughout: triple-z quality for the copper atoms [119] and double-z for main group elements [120] in the case of the studies on interdimeric magnetic interactions. Slight differences in the calculated *J* values (≤1 cm^{-1}) were obtained for *1* and *2* in the diverse calculations carried out by Gaussian on these compounds (even three in the case of *2* before the analysis of the influence of the basis set), depending on the used package. The calculations on different basis sets were carried out using the B3LYP exchange–correlation functional [105,106] and, as indicated in Table 6, the basis sets used are 6-31G(d,p) [121], SDD [122], SV [120], TZVP [119] and LANL2DZ [90,123].

4. Conclusions

Despite the different synthetic methods used because of the reducing character of the I$^-$ ions, the [{CuLX}$_2$] (X = Cl$^-$ and I$^-$) compounds show strong analogies and give rise to S-bridged centrosymmetric dimers that exhibit antiferromagnetic behavior. On the contrary, acid media induce quite different features. The hard Cl$^-$ coligand stabilizes the monomeric [Cu(HL)Cl$_2$]·H$_2$O compound. It contains five-coordinate square-pyramidal Cu(II) ions linked to an NNS tridentate neutral HL ligand. However, the presence of soft iodide ions and non-aqueous highly acid media leads to the attainment of dinuclear [Cu$_2$(H$_2$L)I$_4$] species. They contain tetrahedral Cu(I) ions bonded to cationic monodentate H$_2$L$^+$ lig-

ands through the thioamide S atom, while two iodido ligands act as bridges between the metal centers. As far as we are aware, the coordination polyhedron in this compound exhibits the greatest accumulation of I⁻ ligands reported for any TSC-transition metal complex. Computational calculations reveal a greater thermodynamic stability of the chlorido species in these systems. The attempts to interpret the magnetic properties of the [{CuLX}$_2$] (X = Cl⁻ and I⁻) derivatives through computational methods show a drastic dependence on the chosen basis set for DFT calculations. None of the calculations performed correctly describe the sign and magnitude of the exchange interactions in the iodido **4** dimer. Complementary studies including new computational methodologies are currently underway in order to explain such divergences.

Supplementary Materials: The following supporting information can be downloaded at: https://www.mdpi.com/article/10.3390/inorganics11010031/s1, Figure S1.1: H-bonds (dotted red lines) for compounds **3** (a) and **4** (b); Figure S1.2: π–π Stacking interactions for compounds **3** (a) and **4** (b); Figure S1.3: Anion–π interactions for compounds **3** (a) and **4** (b); Figure S1.4: FTIR-ATR spectra of HL (red), **1** (blue) and **2** (green). Rectangles in black highlight the main differences between the spectra of the free ligand and [{CuLX}$_2$] complexes; Figure S1.5: FTIR ATR spectra of compounds **1** vs. **3**, rectangles frame the A and B regions (see main text); Figure S1.6: FTIR-ATR spectra of HL (red), (H$_2$L)Cl·H$_2$O (green) and **4** (blue). Rectangles in black show bands in the same spectral regions for the three compounds; Figure S1.7: FTIR ATR spectra of compounds **1** vs. **3**, rectangles frame the A and B regions (see main text); Figure S1.8: ESI⁺ mass spectra of compounds **1** (a), **2** (b), **3** (c) and **4** (d), in DMSO solution; Figure S1.9: X-band EPR spectra at RT of compounds **1** (a), **3** (b) and **2** (c). Impurities in **4** (d), whose spectrum has been 120-fold magnified; in dotted lines, the spectrum of **2** for comparative purposes; Figure S1.10: XRD pattern experimental (black) and fitted to the calculated diffractograms of compounds **2** and **4** (red). Figure S2.1: Substitution of aqua ligands with chlorido ones in complex with neutral HL ligand; Figure S2.2: Substitution of aqua ligands with iodido ones in complex with neutral HL ligand; Figure S2.3: Substitution of aqua ligands with chlorido ones in complex with anionic L⁻ ligand; Figure S2.4: Substitution of aqua ligands with iodido ones in complex with anionic L⁻ ligand; Figure S2.5: Different models to evaluate the intermolecular magnetic interactions in the [{CuLBr}$_2$] compound.; Figure S2.6: Experimental χ_m vs. T and χ_mT vs. T for the [{CuLBr}$_2$] compound, together with the corresponding fits χ_m vs. T and χ_mT vs. T considering the J values given on each chart. Table S1.1: Selected hydrogen bonds (Å, °); Table S1.2: Selected IR bands for neutral and anionic thiosemicarbazone derivatives and proposed assignments.

Data Availability Statement: Not applicable.

Conflicts of Interest: The authors declare no conflict of interest.

References

1. Kahn, O. *Molecular Magnetism*; VCH Publishers Inc.: New York, NY, USA, 1993.
2. Campbell, M.J.M. Transition metal complexes of thiosemicarbazide and thiosemicarbazones. *Coord. Chem. Rev.* **1975**, *15*, 279–319. [CrossRef]
3. Agrawal, K.C.; Sartorelli, A.C. Alpha-(N)_Heterocyclic Carboxaldehyde Thiosemicarbazones. In *Handbook of Experimental Pharmacology*; Sartorelli, A.C., Johns, D.G., Eds.; Springer: Berlin, Germany, 1975; pp. 793–807.
4. Sartorelli, A.C.; Agrawal, K.C.; Tsiftsoglou, A.S.; Colleen Moore, E. Characterization of the biochemical mechanism of action of α-(N)-heterocyclic carboxaldehyde thiosemicarbazones. *Adv. Enzym. Regul.* **1977**, *15*, 117–139. [CrossRef]
5. Agrawal, K.C.; Sartorelli, A.C. The Chemistry and Biological Activity of alpha-(N)-Heterocyclic Carboxaldehyde Thiosemicarbazones. *Prog. Med. Chem.* **1978**, *15*, 321–356.
6. Colleen Moore, E.; Sartorelli, A.C. Inhibition of ribonucleotide reductase by α-(N)-heterocyclic carboxaldehyde thiosemicarbazones. *Pharmacol. Ther.* **1984**, *24*, 439–447. [CrossRef]
7. Padhye, S. Transition Metal Complexes of Semicarbazones and Thiosemicarbazones. *Coord. Chem. Rev.* **1985**, *63*, 127–160. [CrossRef]
8. West, D.X.; Padhye, S.B.; Sonawane, P.B. Structural and physical correlations in the biological properties of transition Metal heterocyclic thiosemicarbazone and S-alkyldithiocarbazate complexes. In *Complex Chemistry*; Structure and Bonding; Springer: Berlin, Germany, 1991; Volume 76, pp. 1–50.
9. West, D.X.; Liberta, A.E.; Padhye, S.B.; Chikate, R.C.; Sonawane, P.B.; Kumbhar, A.S.; Yerande, R.G. Thiosemicarbazone complexes of copper (I1): Structural and biological studies. *Coord. Chem. Rev.* **1993**, *123*, 49–71. [CrossRef]
10. Liu, M.-C.; Lin, T.-S.; Sartorelli, A.C. Chemical and Biological Properties of Cytotoxic alpha-(N)-Heterocyclic Carboxaldehyde Thiosemicarbazones. *Prog. Med. Chem.* **1995**, *32*, 1–35.
11. Casas, J.S.; García-Tasende, M.S.; Sordo, J. Main group metal complexes of semicarbazones and thiosemicarbazones. A structural review. *Coord. Chem. Rev.* **2000**, *209*, 197–261. [CrossRef]
12. Blower, P.J.; Castle, T.C.; Cowley, A.R.; Dilworth, J.R.; Donnelly, P.S.; Labisbal, E.; Sowrey, F.E.; Teat, J.; Went, M.J. Structural trends in copper (II) bis (thiosemicarbazone) radiopharmaceuticals. *Dalton Trans.* **2003**, 4416–4425. [CrossRef]
13. Quiroga, A.G.; Navarro Ranninger, C. Contribution to the SAR field of metalated and coordination complexes Studies of the palladium and platinum derivatives with selected thiosemicarbazones as antitumoral drugs. *Coord. Chem. Rev.* **2004**, *248*, 119–133. [CrossRef]
14. Beraldo, H. Semicarbazonas e tiosemicarbazonas: O amplo perfil farmacológico e usos clínicos. *Quim. Nov.* **2004**, *27*, 461–471. [CrossRef]
15. Christlieb, M.; Cowley, A.R.; Dilworth, J.R.; Donnelly, P.S.; Paterson, B.M.; Struthers, H.S.R.; White, J.M. New bimetallic compounds based on the bis(thiosemicarbazonato) motif. *Dalton Trans.* **2007**, 327–331. [CrossRef]
16. Pedrido, R.; Romero, M.J.; Bermejo, M.R.; Martínez-Calvo, M.; González-Noya, A.M.; Zaragoza, G. Coordinative trends of a tridentate thiosemicarbazone ligand: Synthesis, characterization, luminescence studies and desulfurization processes. *Dalton Trans.* **2009**, 8329–8340. [CrossRef]
17. Yu, Y.; Kalinowski, D.S.; Kovacevic, Z.; Siafakas, A.R.; Jansson, P.J.; Stefani, C.; Lovejoy, D.B.; Sharpe, P.C.; Bernhardt, P.V.; Richardson, D.R. Thiosemicarbazones from the old to new: Iron chelators that are more than just ribonucleotide reductase inhibitors. *J. Med. Chem.* **2009**, *52*, 5271–5294. [CrossRef]
18. Lobana, T.S.; Sharma, R.; Bawa, G.; Khanna, S. Bonding and structure trends of thiosemicarbazone derivatives of metals—An overview. *Coord. Chem. Rev.* **2009**, *253*, 977–1055. [CrossRef]
19. Matesanz, A.I.; Souza, P. alpha-N-heterocyclic thiosemicarbazone derivatives as potential antitumor agents: A structure-activity relationships approach. *Mini Rev. Med. Chem.* **2009**, *9*, 1389–1396. [CrossRef]
20. Jansson, P.J.; Sharpe, P.C.; Bernhardt, P.V.; Richardson, D.R. Novel Thiosemicarbazones of the ApT and DpT Series and Their Copper Complexes: Identification of Pronounced Redox Activity and Characterization of Their Antitumor Activity. *J. Med. Chem.* **2010**, *53*, 5759–5769. [CrossRef]
21. Paterson, B.M.; Donnelly, P.S. Copper complexes of bis(thiosemicarbazones): From chemotherapeutics to diagnostic and therapeutic radiopharmaceuticals. *Chem. Soc. Rev.* **2011**, *40*, 3005. [CrossRef]
22. García-Tojal, J.; Gil-García, R.; Gómez-Saiz, P.; Ugalde, M. Pyridine-2-carbaldehyde Thiosemicarbazonecopper System: Extending Some Findings to Other Thiosemicarbazone and Coordination Compounds. *Curr. Inorg. Chem.* **2011**, *1*, 189–210. [CrossRef]
23. Bacher, F.; Enyedy, É.A.; Nagy, N.V.; Rockenbauer, A.; Bognár, G.M.; Trondl, R.; Novak, M.S.; Klapproth, E.; Arion, V.B. Copper(II) Complexes with Highly Water-Soluble L- and D-Proline− Thiosemicarbazone Conjugates as Potential Inhibitors of Topoisomerase IIα. *Inorg. Chem.* **2013**, *52*, 8895–8908. [CrossRef]
24. Park, K.C.; Fouani, L.; Jansson, P.J.; Wooi, D.; Sahni, S.; Lane, D.J.R.; Palanimuthu, D.; Lok, H.C.; Kovačević, Z.; Huang, M.L.H.; et al. Copper and conquer: Copper complexes of di-2-pyridylketone thiosemicarbazones as novel anti-cancer therapeutics. *Metallomics* **2016**, *8*, 874–886. [CrossRef]

25. Pósa, V.; Hajdu, B.; Tóth, G.; Dömötör, O.; Kowol, C.R.; Keppler, B.K.; Spengler, G.; Gyurcsik, B.; Enyedy, É.A. The coordination modes of (thio)semicarbazone copper(II) complexes strongly modulate the solution chemical properties and mechanism of anticancer activity. *J. Inorg. Biochem.* **2022**, *231*, 111786. [CrossRef]

26. Priyarega, S.; Haribabu, J.; Karvembu, R. Development of thiosemicarbazone-based transition metal complexes as homogeneous catalysts for various organic transformations. *Inorg. Chim. Acta* **2022**, *532*, 120742. [CrossRef]

27. Parrilha, G.L.; dos Santos, R.G.; Beraldo, H. Applications of radiocomplexes with thiosemicarbazones and bis(thiosemicarbazones) in diagnostic and therapeutic nuclear medicine. *Coord. Chem. Rev.* **2022**, *458*, 214418. [CrossRef]

28. Antholine, W.E.; Knight, J.M.; Petering, D.H. Some Properties of Copper and Zinc 2-Formylpyridine Thiosemicarbazone. *Inorg. Chem.* **1977**, *16*, 569–574. [CrossRef]

29. Knight, J.M.; Whelan, H.; Petering, D.H. Electronic substituent effects upon properties of 5-substituted-2-formylpyridine thiosemicarbazones and their metal complexes. *J. Inorg. Biochem.* **1979**, *11*, 327–338. [CrossRef]

30. Beraldo, H.; Tosi, L. Spectroscopic studies of metal complexes containing π-delocalized sulfur ligands. The pre-resonance Raman spectra of the antitumor agent 2-formylpyridine thiosemicarbazone and its Cu(II) and Zn(II) complexes. *Inorg. Chim. Acta* **1986**, *125*, 173–182. [CrossRef]

31. Ainscough, E.W.; Brodie, A.M.; Denny, W.A.; Finlay, G.J.; Ranford, J.D. Nitrogen, sulfur and oxygen donor adducts with copper(II) complexes of antitumor 2-formylpyridinethiosemicarbazone analogs: Physicochemical and cytotoxic studies. *J. Inorg. Biochem.* **1998**, *70*, 175–185. [CrossRef]

32. Dömötör, O.; May, N.V.; Pelivan, K.; Kiss, T.; Keppler, B.K.; Kowol, C.R.; Enyedy, É.A. A comparative study of α-N-pyridyl thiosemicarbazones: Spectroscopic properties, solution stability and copper(II) complexation. *Inorg. Chim. Acta* **2018**, *472*, 264–275. [CrossRef]

33. Ainscough, E.W.; Baker, E.N.; Brodie, A.M.; Cresswell, R.J.; Ranford, J.D.; Waters, J.M. The characterization of both the coordinated and non-coordinated saccharinate ion. The syntheses and crystal structures of aqua(2-formylpyridine thiosemicarbazonato)(saccharinato-N)copper(II) hemihydrate and 2,2′-bipyridyl-(2-formylpyridine thiosemicarbaz. *Inorg. Chim. Acta* **1990**, *172*, 185–190. [CrossRef]

34. Ainscough, E.W.; Brodie, A.M.; Ranford, J.D.; Waters, J.M. Reaction of Nitrogen and Sulphur Donor Ligands with the Antiturnour Complex [{CuL(MeCO₂)}₂](HL = 2-formylpyridine thiosemicarbazone) and the single-crystal X-ray structure of [CuL(bipy)]ClO4(bipy = 2,2′-bipyridyl). *J. Chem. Soc. Dalton Trans.* **1991**, 1737–1742. [CrossRef]

35. Gómez-Saiz, P.; García-Tojal, J.; Diez-Gómez, V.; Gil-García, R.; Pizarro, J.L.; Arriortua, M.I.; Rojo, T. Indirect evidences of desulfurization of a thiosemicarbazonecopper(II) system in aqueous basic medium. *Inorg. Chem. Commun.* **2005**, *8*, 259–262. [CrossRef]

36. Ainscough, E.W.; Brodie, A.M.; Ranford, J.D.; Waters, J.M. Preparation and Characterization of Complexes of the Antitumour Copper(II) 2-Formylpyridine Thiosemicarbazone (HL) System and the Single-crystal X-ray Structures of [{Cu(HL)(CF3CO2)}2][CF3CO2]2 and [Cu(HL)(H2O)(ClO4)2].2H2O. *J. Chem. Soc. Dalton Trans.* **1991**, *8*, 2125–2131. [CrossRef]

37. Balakrishnan, N.; Haribabu, J.; Dhanabalan, A.K.; Swaminathan, S.; Sun, S.; Dibwe, D.F.; Bhuvanesh, N.; Awale, S.; Karvembu, R. Thiosemicarbazone(s)-anchored water soluble mono- A nd bimetallic Cu(ii) complexes: Enzyme-like activities, biomolecular interactions, anticancer property and real-time live cytotoxicity. *Dalton Trans.* **2020**, *49*, 9411–9424. [CrossRef]

38. Al-Riyahee, A.A.A.; Horton, P.N.; Coles, S.J.; Amoroso, A.J.; Pope, S. Ni(II), Cu(II) and Zn(II) complexes of functionalised thiosemicarbazone ligands: Syntheses and reactivity, characterization and structural studies. *Polyhedron* **2022**, *225*, 116079. [CrossRef]

39. García-Tojal, J.; Rojo, T. An appraisal of structural, spectroscopic and magnetic aspects of the pyridine-2-carbaldehyde thiosemicarbazonecopper(II) compounds. *Polyhedron* **1999**, *18*, 1123–1130. [CrossRef]

40. Joseph, M.; Suni, V.; Prathapachandra Kurup, M.R.; Nethaji, M.; Kishore, A.; Bhat, S.G. Structural, spectral and antimicrobial studies of copper(II) complexes of 2-benzoylpyridine N(4)-cyclohexyl thiosemicarbazone. *Polyhedron* **2004**, *23*, 3069–3080. [CrossRef]

41. Bleaney, B.; Bowers, K.D. Anomalous Paramagnetism of Copper Acetate. *Proc. R. Soc. Lond. A Math. Phys. Eng. Sci.* **1952**, *214*, 451–465. [CrossRef]

42. Aguirre, M.D.C.; Borrás, J.; Castiñeiras, A.; García-Monteagudo, J.M.; García-Santos, I.; Niclõs, J.; West, D.X. Synthesis, characterization, and properties of some copper(II) complexes of 2-pyridineformamide thiosemicarbazone (HAm4DH). *Eur. J. Inorg. Chem.* **2006**, *2006*, 1231–1244. [CrossRef]

43. Kolotilov, S.V.; Cador, O.; Golhen, S.; Shvets, O.; Ilyin, V.G.; Pavlishchuk, V.V.; Ouahab, L. Synthesis, structure, sorption and magnetic properties of Ni(II) and Cu(II) complexes with thiosemicarbazone of 2-hydroxybenzaldehyde, bridged by 4,4′-bipyridine. *Inorg. Chim. Acta* **2007**, *360*, 1883–1889. [CrossRef]

44. Revenko, M.D.; Bourosh, P.N.; Stratulat, E.F.; Gdaniec, M.; Lipkowski, Y.; Korzha, I.D.; Simonov, Y.A. Synthesis and structure of copper(II) coordination compounds with 8-quinolinecarboxaldehyde thio- and 4-phenylthiosemicarbazones. *Russ. J. Inorg. Chem.* **2010**, *55*, 1387–1397. [CrossRef]

45. Revenco, M.D.; Palamarciuc, O.V.; Bourosh, P.N.; Lipkowski, J.; Gdaniec, M.; Simonov, Y.A.; Clérac, R. New template reactions of salicylaldehyde S-methyl-isothiosemicarbazone with 2-formylpyridine promoted by Ni(II) or Cu(II) metal ions. *Inorg. Chim. Acta* **2011**, *368*, 157–164. [CrossRef]

46. Saha, N.C.; Pradhan, R.; Das, M.; Khatun, N.; Mitra, D.; Samanta, A.; Slawin, A.M.Z.; Jana, A.D.; Klanke, J.; Rentschler, E. Synthesis, characterization, X-ray crystallography, and antimicrobial activities of Ni (II) and Cu (II) complexes with a salicylaldehyde-based thiosemicarbazone ligand. *J. Coord. Chem.* **2014**, *67*, 286–299. [CrossRef]

47. Uraev, A.I.; Nefedov, S.E.; Lyssenko, K.A.; Vlasenko, V.G.; Ikorskii, V.N.; Garnovskii, D.A.; Makarova, N.I.; Levchenkov, S.I.; Shcherbakov, I.N.; Milenkovic, M.R.; et al. Synthesis, structure, spectroscopic studies and magnetic based on aminomethylene derivatives of pyrazole-5-one (thione). *Poly* **2020**, *188*, 114623. [CrossRef]

48. Novoa, N.; Justaud, F.; Hamon, P.; Roisnel, T.; Cador, O.; Le Guennic, B.; Manzur, C.; Carrillo, D.; Hamon, J.R. Doubly phenoxide-bridged binuclear copper(II) complexes with ono tridentate schiff base ligand: Synthesis, structural, magnetic and theoretical studies Dedicated to Dr. Claude Lapinte for his outstanding contribution to organometallic molecular wires. *Polyhedron* **2015**, *86*, 81–88. [CrossRef]

49. Bazhin, D.N.; Kudyakova, Y.S.; Slepukhin, P.A.; Burgart, Y.V.; Malysheva, N.N.; Kozitsina, A.N.; Ivanova, A.V.; Bogomyakov, A.S.; Saloutin, V.I. Dinuclear copper(ii) complex with novel N,N′,N″,O-tetradentate Schiff base ligand containing trifluoromethylpyrazole and hydrazone moieties. *Mendeleev Commun.* **2018**, *28*, 202–204. [CrossRef]

50. Peña, Q.; Sciortino, G.; Maréchal, J.-D.; Bertaina, S.; Simaan, A.J.; Lorenzo, J.; Capdevila, M.; Bayón, P.; Iranzo, O.; Palacios, O. Copper(II) N,N,O-Chelating Complexes as Potential Anticancer Agents. *Inorg. Chem.* **2021**, *60*, 2939–2952. [CrossRef]

51. Gil-García, R.; Gómez-Saiz, P.; Díez-Gómez, V.; Madariaga, G.; Insausti, M.; Lezama, L.; Vicente, J.; García-Tojal, J. Thiosemicarbazonecopper(II) compounds with halide/hexafluorosilicate anions: Structure, water clusters, non-covalent interactions and magnetism. *Polyhedron* **2014**, *81*, 675–686. [CrossRef]

52. Gómez-Saiz, P.; García-Tojal, J.; Mendia, A.; Donnadieu, B.; Lezama, L.; Pizarro, J.L.; Arriortua, M.I.; Rojo, T. Coordination Modes in a Tridentate NNS (Thiosemicarbazonato)copper(II) System Containing Oxygen-Donor Coligands—Structures of [{Cu(L)(X)}2] (X = Formato, Propionato, Nitrito). *Eur. J. Inorg. Chem.* **2003**, *3*, 518–527. [CrossRef]

53. Gil-García, R.; Gómez-Saiz, P.; Díez-Gómez, V.; Donnadieu, B.; Insausti, M.; Lezama, L.; García-Tojal, J. Polymorphism and magnetic properties in thiosemicarbazonecopper(II)-sulfate compounds. *Polyhedron* **2013**, *54*, 243–251. [CrossRef]

54. García-Tojal, J.; Urtiaga, M.K.; Cortés, R.; Lezama, L.; Rojo, T.; Arriortua, M.I. Synthesis, structure, spectroscopic and magnetic properties of two copper(II) dimers containing pyridine-2-carbaldehyde thiosemicarbazonate (L), [{CuL(X)}2](X = Cl or Br). *J. Chem. Soc. Dalton Trans.* **1994**, *15*, 2233–2238. [CrossRef]

55. Gómez-Saiz, P.; Gil-García, R.; Maestro, M.A.; Pizarro, J.L.; Arriortua, M.I.; Lezama, L.; Rojo, T.; González-Álvarez, M.; Borrás, J.; García-Tojal, J. Structure, magnetic properties and nuclease activity of pyridine-2-carbaldehyde thiosemicarbazonecopper(II) complexes. *J. Inorg. Biochem.* **2008**, *102*, 1910–1920. [CrossRef] [PubMed]

56. García-Tojal, J.; Lezama, L.; Pizarro, J.L.; Insausti, M.; Arriortua, M.I.; Rojo, T. Spectroscopic and magnetic properties of copper(II) complexes derived from pyridine-2-carbaldehyde thiosemicarbazone. Structures of [Cu(NO3)(C7H8N4S)(H2O)](NO3) and [{Cu(NCS)(C7H7N4S)}2]. *Polyhedron* **1999**, *18*, 3703–3711. [CrossRef]

57. Gómez-Saiz, P.; García-Tojal, J.; Maestro, M.A.; Mahía, J.; Arnáiz, F.J.; Lezama, L.; Rojo, T. New 1,3,4-Oxadiazolecopper(II) Derivatives Obtained from Thiosemicarbazone Complexes. *Eur. J. Inorg. Chem.* **2003**, *14*, 2639–2650. [CrossRef]

58. Gómez-Saiz, P.; García-Tojal, J.; Maestro, M.A.; Arnaiz, F.J.; Rojo, T. Evidence of Desulfurization in the Oxidative Cyclization of Thiosemicarbazones. Conversion to 1,3,4-Oxadiazole Derivatives. *Inorg. Chem.* **2002**, *41*, 1345–1347. [CrossRef]

59. Bingham, A.G.; Bögge, H.; Müller, A.; Ainscough, E.W.; Brodie, A.M. Synthetic, Spectroscopic, and X-ray Crystallographic Studies on Binuclear Copper(II) Complexes with a Tridentate NNS-bonding 2-Formylpyridine Thiosemicarbazone Ligand. The Characterization of Both Neutral and Deprotonated Co-ordinated Ligand Structures. *J. Chem. Soc. Dalton Trans.* **1987**, *3*, 493–499. [CrossRef]

60. Ainscough, E.W.; Brodie, M.; Ranford, J.D.; Waters, J.M.; Murray, K.S. The reaction of the pyrophosphate ion with the antitumour [{CuL(CH3COO)}2] (HL = 2-formylpyridine thiosemicarbazone) the single-crystal X-ray structure of [(CuL)4P2O7] ·NH2O. *Inorg. Chim. Acta* **1992**, *197*, 107–115. [CrossRef]

61. Lobana, T.S.; Khanna, S.; Butcher, R.J. 2-Benzoylpyridine thiosemicarbazone as a novel reagent for the single pot synthesis of dinuclear CuI–CuII complexes: Formation of stable copper(ii)–iodide bonds. *Dalton Trans.* **2012**, *41*, 4845–4851. [CrossRef]

62. Kumar, S.M.; Dhahagani, K.; Rajesh, J.; Anitha, K.; Chakkaravarthi, G.; Kanakachalam, N.; Marappan, M.; Rajagopal, G. Synthesis, structural analysis and cytotoxic effect of copper (II) -thiosemicarbazone complexes having heterocyclic bases: A selective naked eye sensor for F À and CN À. *Polyhedron* **2015**, *85*, 830–840. [CrossRef]

63. Jayakumar, K.; Sithambaresan, M.; Aiswarya, N.; Kurup, M.R.P. Spectrochimica Acta Part A: Molecular and Biomolecular Spectroscopy Synthesis and spectral characterization of mono- and binuclear thiosemicarbazone: Crystal structure of a novel sulfur bridged copper (II). *Spectrochim. Acta Part A Mol. Biomol. Spectrosc.* **2015**, *139*, 28–36. [CrossRef]

64. Indoria, S.; Lobana, T.S.; Singh, D.; Kumari, S.; Kumari, P.; Bala, T.; Kamal, A.; Jassal, A.K.; García Santos, I.; Castineiras, A.; et al. Stabilization of Cu[II]-I Bonds Using 2-Benzoylpyridine Thiosemicarbazones—Synthesis, Structure, Spectroscopy, Fluorescence, and Cyclic Voltammetry. *Eur. J. Inorg. Chem.* **2015**, *2015*, 5106–5117. [CrossRef]

65. Kaushal, M.; Lobana, T.S.; Nim, L.; Kaur, J.; Bala, R.; Hundal, G.; Arora, D.S.; Garcia-Santos, I.; Duff, C.E.; Jasinski, J.P. Synthesis, structures, antimicrobial activity and biosafety evaluation of pyridine-2-formaldehyde-N-susbtituted-thiosemicarbazonates of copper(ii). *New J. Chem.* **2018**, *42*, 15879–15894. [CrossRef]

66.	Tom, L.; Aiswarya, N.; Sreejith, S.S.; Kurup, M.R.P. Self-organized three dimensional architectures based on non-covalent interactions in square planar Cu(II) thiosemicarbazone: Solvent mediated crystallization and EPR based correlation study. *Inorg. Chim. Acta* **2018**, *473*, 223–235. [CrossRef]

67.	Kaushal, M.; Lobana, T.S.; Nim, L.; Bala, R.; Arora, D.S.; Garcia-Santos, I.; Duff, C.E.; Jasinski, J.P. Synthesis of 2-acetylpyridine-N -substituted thiosemicarbazonates of copper(ii) with high antimicrobial activity against methicillin resistant *S. aureus*, *K. pneumoniae* 1 and *C. albicans*. *New J. Chem.* **2019**, *43*, 11727–11742. [CrossRef]

68.	Jin, J.; Hu, J.; Qin, Y.; Zhang, J.; Zhao, J.; Yue, L.; Hou, H. In vitro and in vivo anticancer activity of a thiourea tripyridyl dinuclear Cu(ii) complex. *New J. Chem.* **2019**, *43*, 19286–19297. [CrossRef]

69.	Lobana, T.S.; Kaushal, M.; Bala, R.; Nim, L.; Paul, K.; Arora, D.S.; Bhatia, A.; Arora, S.; Jasinski, J.P. Di-2-pyridylketone-N1-substituted thiosemicarbazone derivatives of copper(II): Biosafe antimicrobial potential and high anticancer activity against immortalized L6 rat skeletal muscle cells. *J. Inorg. Biochem.* **2020**, *212*, 111205. [CrossRef] [PubMed]

70.	Calvary, C.A.; Hietsoi, O.; Hofsommer, D.T.; Brun, H.C.; Costello, A.M.; Mashuta, M.S.; Spurgeon, J.M.; Buchanan, R.M.; Grapperhaus, C.A. Copper bis(thiosemicarbazone) Complexes with Pendent Polyamines: Effects of Proton Relays and Charged Moieties on Electrocatalytic HER. *Eur. J. Inorg. Chem.* **2021**, *2021*, 267–275. [CrossRef]

71.	Mohan, B.; Choudhary, M. Synthesis, crystal structure, computational study and anti-virus effect of mixed ligand copper (II) complex with ONS donor Schiff base and 1, 10-phenanthroline. *J. Mol. Struct.* **2021**, *1246*, 131246. [CrossRef] [PubMed]

72.	García-Tojal, J.; García-Jaca, J.; Cortés, R.; Rojo, T.; Urtiaga, M.K.; Arriortua, M.I. Synthesis and spectroscopic properties of two pyridine-2-carbaldehyde thiosemicarbazonecopper(II) compounds: [CuX$_2$(C$_7$H$_8$N$_4$S)]. H$_2$0 (X = Br, Cl). Crystal structure of the bromo complex. *Inorg. Chim. Acta* **1996**, *249*, 25–32. [CrossRef]

73.	Addison, A.W.; Rao, T.N.; Reedijk, J.; van Rijn, J.; Verschoor, G.C. Synthesis, Structure, and Spectroscopic Properties of Copper(II) Compounds containing Nitrogen-Sulphur Donor Ligands; the Crystal and Molecular Structure of Aqua[1,7-bis(N-methylbenzimidazol-2′-yl)- 2,6-dithiaheptane]copper(II) Perchlorate. *J. Chem. Soc. Dalton Trans.* **1984**, 1349–1356. [CrossRef]

74.	Gil-García, R.; Zichner, R.; Díez-Gómez, V.; Donnadieu, B.; Madariaga, G.; Insausti, M.; Lezama, L.; Vitoria, P.; Pedrosa, M.R.; García-Tojal, J. Polyoxometallate-thiosemicarbazone hybrid compounds. *Eur. J. Inorg. Chem.* **2010**, *2010*, 4513–4525. [CrossRef]

75.	Gatto, C.C.; Lima, F.C.; Miguel, P.M. Copper(II) complexes with semicarbazones: Synthesis, characterization and noncovalent interactions in their crystal structures. *J. Chem. Sci.* **2020**, *132*, 146. [CrossRef]

76.	Yang, L.; Powell, D.R.; Houser, R.P. Structural variation in copper(I) complexes with pyridylmethylamide ligands: Structural analysis with a new four-coordinate geometry index, tau4. *Dalton Trans.* **2007**, 955–964. [CrossRef] [PubMed]

77.	Urtiaga, M.K.; Arriortua, M.I.; García-Tojal, J.; Rojo, T. Pyridine-2-carbaldehyde thiosemicarbazone hydrochloride monohydrate, 2C$_7$H$_9$N$_4$S$^+$.2Cl$^-$.2H$_2$O. *Acta Crystallogr.* **1995**, *C51*, 2172–2174. [CrossRef]

78.	Morsali, A.; Ramazani, A.; Jamali, F.; Gouranlou, F. Crystal structure of pyridine-2-carbaldehyde thiosemicarbazonium perchlorate, (C$_7$H$_9$N$_4$S)(ClO$_4$). *Z. Kristallogr. NCS* **2001**, *216*, 607–608. [CrossRef]

79.	Biyushkin, V.N.; Chumakov, Y.N.; Samus, N.M.; Baka, I.O. Molecular structure and electronic structure of 2-pyridine-carbaldehyde thiosemicarbazone. *J. Struct. Chem.* **1987**, *28*, 119–121. [CrossRef]

80.	Taishang, H. Synthesis and molecular structure determination of 2-formylpyridine thiosemicarbazone. *J. Xiamen Univ.* **1993**, *52*, 741–744.

81.	Jin, Z.M.; Shen, L.; He, L.; Guo, H.; Wang, H.T. Pyridine-2-carbaldehyde thiosemicarbazone 1.75 hydrate. *Acta Crystallogr.* **2003**, *E59*, o1909–o1911. [CrossRef]

82.	López-Torres, E.; Mendiola, M.A. Mercury complexes with the ligand benzaldehyde-N(4),N(4)-dimethylthiosemicarbazone. *Inorg. Chim. Acta* **2010**, *363*, 1275–1283. [CrossRef]

83.	Fathy, A.; Ibrahim, A.B.M.; Elkhalik, S.A.; Meurer, F.; Bodensteiner, M.; Abbas, S.M. Thiosemicarbazones and derived antimony complexes: Synthesis, structural analysis, and in vitro evaluation against bacterial, fungal and cancer cells. *Inorganics* **2022**, *10*, 172. [CrossRef]

84.	Bell, C.F.; Lott, K.A.K.; Hearn, N. Copper complexes of pyridine 2-aldehyde and 2-acetylpyridine thiosemicarbazones. *Polyhedron* **1987**, *6*, 39–44. [CrossRef]

85.	Lobana, T.S.; Rekha; Butcher, R.J.; Castiñeiras, A.; Bermejo, E.; Bharatam, P.V. Bonding Trends of Thiosemicarbazones in Mononuclear and Dinuclear Copper(I) Complexes: Syntheses, Structures, and Theoretical Aspects. *Inorg. Chem.* **2006**, *45*, 1535–1542. [CrossRef] [PubMed]

86.	Lobana, T.S.; Sharma, R.; Castineiras, A.; Hundal, G.; Butcher, R.J. The influence of substituents (R) at N1 atom of thiophene-2-carbaldehyde thiosemicarbazones {(C4H3S)HC2{double bond, long}N3-N(H)-C1({double bond, long}S)N1HR} on bonding, nuclearity and H-bonded networks of copper(I) complexes. *Inorg. Chim. Acta* **2009**, *362*, 3547–3554. [CrossRef]

87.	Sharma, R.; Lobana, T.S.; Castineiras, A.; Butcher, R.J.; Akitsu, T. The influence of substituents at C 2 / N 1 atoms of pyridine-2-type of copper (I) complexes. *Polyhedron* **2019**, *158*, 449–457. [CrossRef]

88.	Ibrahim, A.B.M.; Farh, M.K.; Mayer, P. Copper complexes of new thiosemicarbazone ligands: Synthesis, structural studies and antimicrobial activity. *Inorg. Chem. Commun.* **2018**, *94*, 127–132. [CrossRef]

89.	Venegas-Yazigi, D.; Aravena, D.; Spodine, E.; Ruiz, E.; Alvarez, S. Structural and electronic effects on the exchange interactions in dinuclear bis (phenoxo) -bridged copper (II) complexes. *Coord. Chem. Rev.* **2010**, *254*, 2086–2095. [CrossRef]

90. Naskar, S.; Naskar, S.; Mayer-Figge, H.; Sheldrick, W.S.; Corbella, M.; Tercero, J.; Chattopadhyay, S.K. Study of copper(II) complexes of two diacetyl monooxime thiosemicarbazones: X-ray crystal structure and magneto-structural correlation of [Cu(dmoTSCH)Cl] 2·H 2O (dmoTSCH = monoanion of diacetyl monooxime thiosemicarbazone). *Polyhedron* **2012**, *35*, 77–86. [CrossRef]

91. Gómez-Saiz, P.; García-Tojal, J.; Maestro, M.; Mahía, J.; Lezama, L.; Rojo, T. Coordination modes in a (thiosemicar-bazone)copper(II)/oxalato system—Structures of [{Cu(L)}₂(ox)]·2H₂O, [Cu(HL)(ox)(H₂O)], [{Cu(HL)}₂(ox)]-[Cu(ox)₂]·2H₂O and [{Cu(HL)}₂(ox)](NO₃)₂. *Eur. J. Inorg. Chem.* **2003**, *2003*, 2123–2132. [CrossRef]

92. Ruiz, E.; Cano, J.; Alvarez, S.; Alemany, P. Broken symmetry approach to calculation of exchange coupling constants for homobinuclear and heterobinuclear transition metal complexes. *J. Comput. Chem.* **1999**, *20*, 1391–1400. [CrossRef]

93. Soler, J.M.; Artacho, M.; Gale, J.D.; García, A.; Junquera, J.; Ordejón, P.; Sánchez-Portal, D. The SIESTA method for ab initio order-N materials simulation. *J. Phys. Condens. Matter* **2002**, *14*, 2745–2779. [CrossRef]

94. Kresse, G.; Hafner, J. Ab initio molecular dynamics for liquid metals. *Phys. Rev. B* **1993**, *47*, 558–561. [CrossRef] [PubMed]

95. Kresse, G.; Furthmüller, J. Efficient iterative schemes for ab initio total-energy calculations using a plane-wave basis set. *Phys. Rev. B* **1996**, *54*, 11169–11186. [CrossRef] [PubMed]

96. Perdew, J.P.; Burke, K.; Ernzerhof, M. Generalized Gradient Approximation Made Simple. *Phys. Rev. Lett.* **1996**, *77*, 3865–3868. [CrossRef] [PubMed]

97. Neese, F. Prediction of molecular properties and molecular spectroscopy with density functional theory: From fundamental theory to exchange-coupling. *Coord. Chem. Rev.* **2009**, *253*, 526–563. [CrossRef]

98. Soek, R.N.; Tiago, T.L.; Garbelini, E.R.; Crespan, E.d.R.; Pineider, F.; Poneti, G.; Machado, G.S.; Ribeiro, R.R.; Hörner, M.; Nunes, F.S. Structural, Magnetic, Spectroscopic and Density Functional Theory (DFT) Analysis of Bis((1-((E)-2-pyridinylmethylidene)semicarbazone)copper(II)sulfate) Dihydrate Complex. *ChemistrySelect* **2017**, *2*, 8451–8458. [CrossRef]

99. Anderson, F.E.; Duca, C.J.; Scudi, J.V. Some heterocyclic thiosemicarbazones. *J. Am. Chem. Soc.* **1951**, *73*, 4967–4968. [CrossRef]

100. *WINEPR SimFonia, version 1.25*; Bruker Analytische Messtecnik GmβH: Rheinstetten, Germany, 1996.

101. *X-Area, Software Manual*; STOE & Cie Gmbh: Darmstadt, Germany, 2015.

102. Altomare, A.; Burla, M.C.; Camalli, M.; Cascarano, G.L.; Giacovazzo, C.; Guagliardi, A.; Moliterni, A.G.G.; Polidori, G.; Spagna, R. SIR97: A new tool for crystal structure determination and refinement. *J. Appl. Crystallogr.* **1999**, *32*, 115–119. [CrossRef]

103. Sheldrick, G.M. SHELXT—Integrated space-group and crystal-structure determination. *Acta Crystallogr.* **2015**, *C71*, 3–8. [CrossRef] [PubMed]

104. Farrugia, L.J. WinGX and ORTEP for Windows: An update. *J. Appl. Crystallogr.* **2012**, *45*, 849–854. [CrossRef]

105. Becke, A.D. Density functional thermochemistry. 3.The role of exact exchange. *J. Chem. Phys.* **1993**, *98*, 5648–5652. [CrossRef]

106. Lee, C.T.; Yang, W.T.; Parr, R.G. Development of the Colle-Salvetti correlation-energy formula into a functional of the electron-density. *Phys. Rev. B* **1988**, *37*, 785–789. [CrossRef] [PubMed]

107. Neese, F. The ORCA program system. *WIREs Comput. Mol. Sci.* **2012**, *2*, 73–78. [CrossRef]

108. Neese, F. Software update: The ORCA program system, version 4.0. *WIREs Comput. Mol. Sci.* **2018**, *8*, e1327. [CrossRef]

109. Weigend, F.; Ahlrichs, R. Balanced basis sets of split valence, triple zeta valence and quadruple zeta valence quality for H to Rn: Design and assessment of accuracy. *Phys. Chem. Chem. Phys.* **2005**, *7*, 3297–3305. [CrossRef]

110. Weigend, F. Accurate Coulomb-fitting basis sets for H to Rn. *Phys. Chem. Chem. Phys.* **2006**, *8*, 1057. [CrossRef]

111. Marenich, A.V.; Cramer, C.J.; Truhlar, D.G. Universal Solvation Model Based on Solute Electron Density and on a Continuum Model of the Solvent Defined by the Bulk Dielectric Constant and Atomic Surface Tensions. *J. Phys. Chem. B* **2009**, *113*, 6378–6396. [CrossRef]

112. Ruiz, E.; Alemany, P.; Alvarez, S.; Cano, J. Toward the prediction of magnetic coupling in molecular systems: Hydroxo- and alkoxo-bridged Cu(II) binuclear complexes. *J. Am. Chem. Soc.* **1997**, *119*, 1297–1303. [CrossRef]

113. Ruiz, E.; Rodríguez-Fortea, A.; Cano, J.; Alvarez, S.; Alemany, P. About the calculation of exchange coupling constants in polynuclear transition metal complexes. *J. Comput. Chem.* **2003**, *24*, 982–989. [CrossRef]

114. Frisch, M.J.; Trucks, G.W.; Schlegel, H.B.; Scuseria, G.E.; Robb, M.A.; Cheeseman, J.R.; Montgomery, J.A.; Vreven, T.; Kudin, K.N.; Burant, J.C.; et al. *Gaussian 03, revision B.4*; Carnegie Mellon University: Pittsburgh, PA, USA, 2003.

115. Frisch, M.J.; Trucks, G.W.; Schlegel, H.B.; Scuseria, G.E.; Robb, M.A.; Cheeseman, J.R.; Scalmani, G.; Barone, V.; Mennucci, B.; Petersson, G.A.; et al. *Gaussian 09, revision D.01*; Gaussian Inc.: Wallingford, CT, USA, 2013.

116. Becke, A.D. Density-functional exchange energy approximation with correct asymptotic behavior. *Phys. Rev. A* **1988**, *38*, 3098–3100. [CrossRef]

117. Ruiz, E.; Cano, J.; Alvarez, S.; Alemany, P. Magnetic coupling in end-on azido-bridged transition metal complexes: A density functional study. *J. Am. Chem. Soc.* **1998**, *120*, 11122–11129. [CrossRef]

118. Ruiz, E.; Alvarez, S.; Rodríguez-Fortea, A.; Alemany, P.; Pouillon, Y.; Massobrio, C. Electronic Structure and Magnetic Behavior in Polynuclear Transition-metal Compounds. In *Magnetism: Molecules to Materials II: Models and Experiments*; Miller, J.S., Drillon, M., Eds.; Wiley-VCH: Weinheim, Germany, 2001.

119. Schäfer, A.; Huber, C.; Ahlrichs, R. Fully optimized contracted Gaussian basis sets of triple zeta valence quality for atoms Li to Kr. *J. Chem. Phys.* **1994**, *100*, 5829–5835. [CrossRef]

120. Schäfer, A.; Horn, H.; Ahlrichs, R. Fully optimized contracted Gaussian basis sets for atoms Li to Kr. *J. Chem. Phys.* **1992**, *97*, 2571–2577. [CrossRef]

121. Hehre, W.J.; Ditchfield, R.; Pople, J.A. Self—Consistent Molecular Orbital Methods. XII. Further Extensions of Gaussian—Type Basis Sets for Use in Molecular Orbital Studies of Organic Molecules. *J. Chem. Phys.* **1972**, *56*, 2257–2261. [CrossRef]
122. Dolg, M.; Wedig, U.; Stoll, H.; Preuss, H. Energy-adjusted a b i n i t i o pseudopotentials for the first row transition elements. *J. Chem. Phys.* **1987**, *86*, 866–872. [CrossRef]
123. Hay, P.J.; Wadt, W.R. Ab initio effective core potentials for molecular calculations. Potentials for K to Au including the outermost core orbitals. *J. Chem. Phys.* **1985**, *82*, 299–310. [CrossRef]